2021

Master's thesis

3D MRI Reconstruction Based on 2D Generative Adversarial Network Super-Resolution

1237001 Zhang Hongtao

Advisor Professor Yoshida Shinichi

August 6, 2021

Informatics Course

Graduate School of Engineering, Kochi University of Technology

Abstract

3D MRI Reconstruction Based on 2D Generative Adversarial Network Super-Resolution

Zhang Hongtao

In medical diagnosis, the diagnosis of brain pathology often requires the analysis of the brain through imaging. MRI is currently one of the mainstream brain imaging techniques. The image quality of brain MRI generally depends on the strength of the static magnetic field. MRI Scanners with lower field strength have disadvantages such as low resolution, high imaging cost, and long scanning time. Researchers used an iterative method to solve the problem and reconstruct MRI images through prior information. With the in-depth development of machine learning, deep learning models for super-resolution reconstruction of MRI images have become a mainstream trend. Nowadays, the traditional deep learning-based super-resolution method uses a three-dimensional convolutional neural network to reconstruct MRI images, thereby obtaining high-resolution MRI images. However, there is a problem of higher training costs. Our research proposes using two-dimensional generative adversarial neural network technology for super-resolution reconstruction of MRI images. In the experiment, we design two reconstruction steps. In advance of the reconstruction steps, based on the three-dimensional peculiarities of MRI and a scale factor of 2, we simulate half of the MRI slice volume as input. In the first step, we use the residual multi-scale module attention mechanism generative adversarial network (RMAM-GAN) to reconstruct the MRI image. RMAM-GAN is a two dimensional generative adversarial network and is

superior to other super-resolution technologies in texture and frequency information. Then we stack the reconstructed MRI images and rebuild them to new MRI. The reconstructed MRI consists of only half of the slices, and there are still missing values and noise. Using the traditional interpolation method will enlarge the influence of the noise area. Therefore, we propose a noise-based enhanced super-resolution generative adversarial network (nESRGAN) in the second reconstruction. The noise added to the network can provide additional texture restoration possibilities. We use nESRGAN to restore MRI resolution and high-frequency details further. Finally, we achieve the 3D reconstruction of brain MRI through two generative adversarial networks. Our proposed method is superior to 3D super-resolution technology based on deep learning regarding perception range and image quality evaluation criteria.

key words magnetic resonance imaging; deep learning; super-resolution; three-dimensional reconstruction; RMAM-GAN; nESRGAN

Contents

List of Figures

List of Tables

Chapter 1

Introduction

In this chapter, we mainly introduce the experimental background and the mainstream networks under deep learning. In addition, we also review the development of MRI in the direction of super-resolution and introduce the main contributions and significance of the experiment.

1.1 Background

The analysis of brain pathology has always been an active area of research. Through brain imaging, information about brain diseases can be obtained, which is helpful to the prevention and early diagnosis of brain diseases[1]. Magnetic resonance imaging (MRI) is one of the most important diagnostic imaging methods widely used in the diagnosis and image-guided therapy, especially brain imaging diagnosis[2]. The quality of MRI images is generally determined by the field strength and signal of the MRI scanner. High-quality images often require more time cost and a smaller signal-to-noise ratio. At present, most of the MRI scanners commonly used in hospitals are scanners with a field strength of 1.5 Tesla[3][4]. In a limited time, MRI images have the characteristics of low resolution, and there are also limiting factors such as long imaging time and noise. Due to the limitations of imaging technology[5], image super-resolution technology is favored by medical experts. Image super-resolution technology refers to reconstructing input low-resolution images into high-resolution images through specific algorithms and

processing methods[6][7].

Researchers have used three-dimensional convolutional neural networks (3DCNN)[8] to perform MRI super-resolution reconstruction in recent years. 3DCNN can directly extract 3D image features to reconstruct the entire MRI. Nevertheless, there are problems such as a large amount of calculation and high time cost. Therefore, we propose using two-dimensional convolutional neural networks to reduce memory allocation and time costs.

Our research uses deep learning-based super-resolution models to perform 3D reconstruction of MRI. The experiment adopts the characteristics of MRI in two-dimensional slices[9] and prepares two-step reconstruction, respectively. The first reconstruction mainly restores the high-frequency information of MRI and then reorganizes it. After the rebuilding, the second reconstruction solves the missing value and noise problems and finally obtains a high-resolution MRI. Our proposed method is superior to 3D Convolutional Neural Network in terms of vision and image evaluation. The high-resolution MRI images obtained can support an effiective and accurate diagnosis of a medical doctor within a limited time.

1.2 Deep Learning

1.2.1 Convolution Neural Network

The super-resolution method based on CNN, means that after the pixels are copied and magnified, a specific fixed convolution kernel is used to convolve and learn this convolution kernel.

According to the convolutional neural network characteristics, CNN can obtain high-frequency information from images and can learn nonlinear relationships. Then low-resolution images and high-resolution images can be fitted through nonlinear map-

ping. It updates the network parameters according to the difference between the constructed super-resolution image and the actual high-resolution image. CNN uses the traditional loss function to measure the accuracy of the image, and the mathematical proximity is used to measure the smooth average of the colors in the area of the image. The visually generated image is sometimes not close to the actual image. The primary process is shown in Figure 1.1.

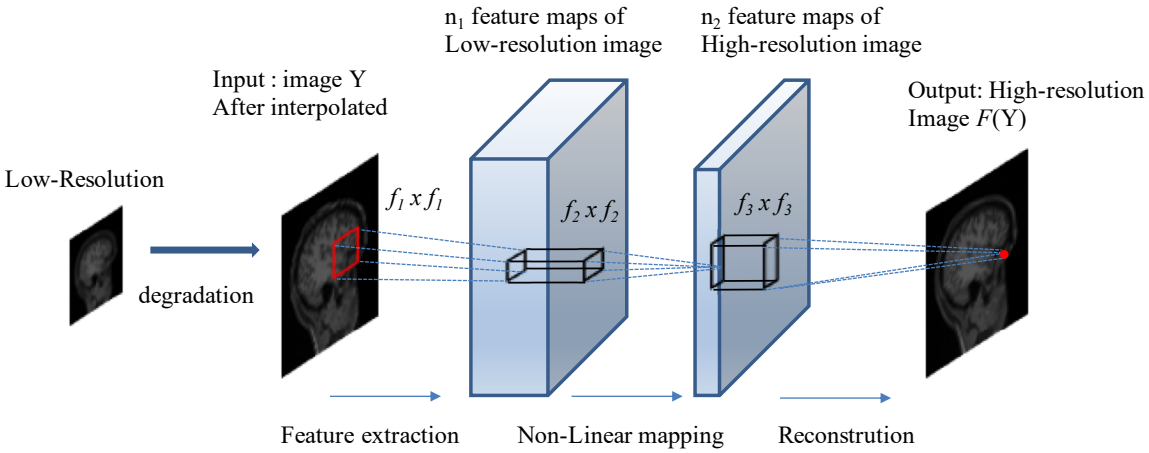

Fig. 1.1 MRI super-resolution in CNN.

1.2.2 Generative Adversarial Network

Unlike CNN, a generative adversarial network(GAN) adopts the idea of game confrontation and uses adversarial loss and content loss. There have some benefits of GAN. One of the great benefits is that GAN can use the adversarial loss to encourage the output to look natural. The adversarial loss is part of the discriminator network's evaluation of the generator's operating conditions. If the discriminator believes that the image makes the generator look reliable, the loss is less than the loss that the image is ultimately forged. The content loss compares the fine details in the image by passing the generated image and the original image through the

CNN feature map and calculating the output loss. GAN combines perceptual loss with generative loss and applies sub-pixel convolution for up-sampling, generating better photo-realistic super-resolution images. The primary process is shown in Figure 1.2.

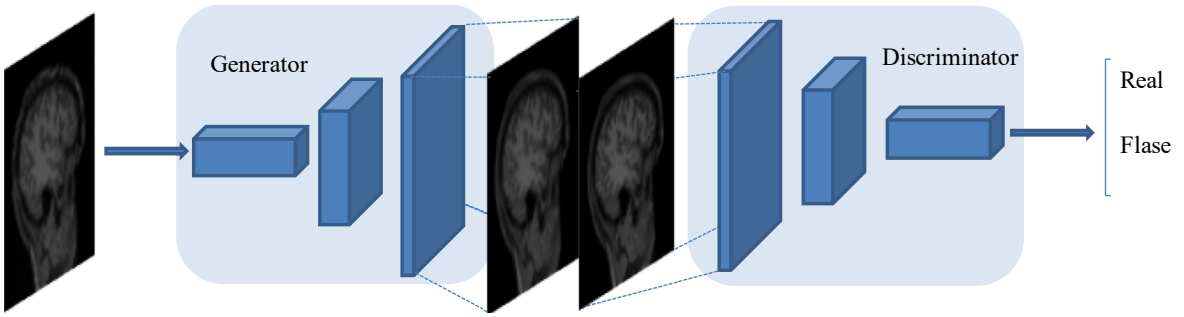

Fig. 1.2 MRI super-resolution in GAN.

1.3 MRI in Super Resolution

1.3.1 Super Resolution Reconstruction

Early super-resolution research on MRI images used super-resolution reconstruction (SRR) to improve the resolution of MRI images[10][11][12]. The SRR algorithm can mine the relative motion relationship between low-resolution images or video sequences and mix this relationship on a frame, thereby improving the image's resolution. At first, MRI image reconstruction based on super-resolution technology initially adopted the spatial method. High-resolution images are reconstructed using a series of low-resolution images with different spatial displacements or blur degrees and some preliminary information. However, the disadvantage is that the model is complex, and the calculation is extensive. The main idea is shown in Figure 1.3.

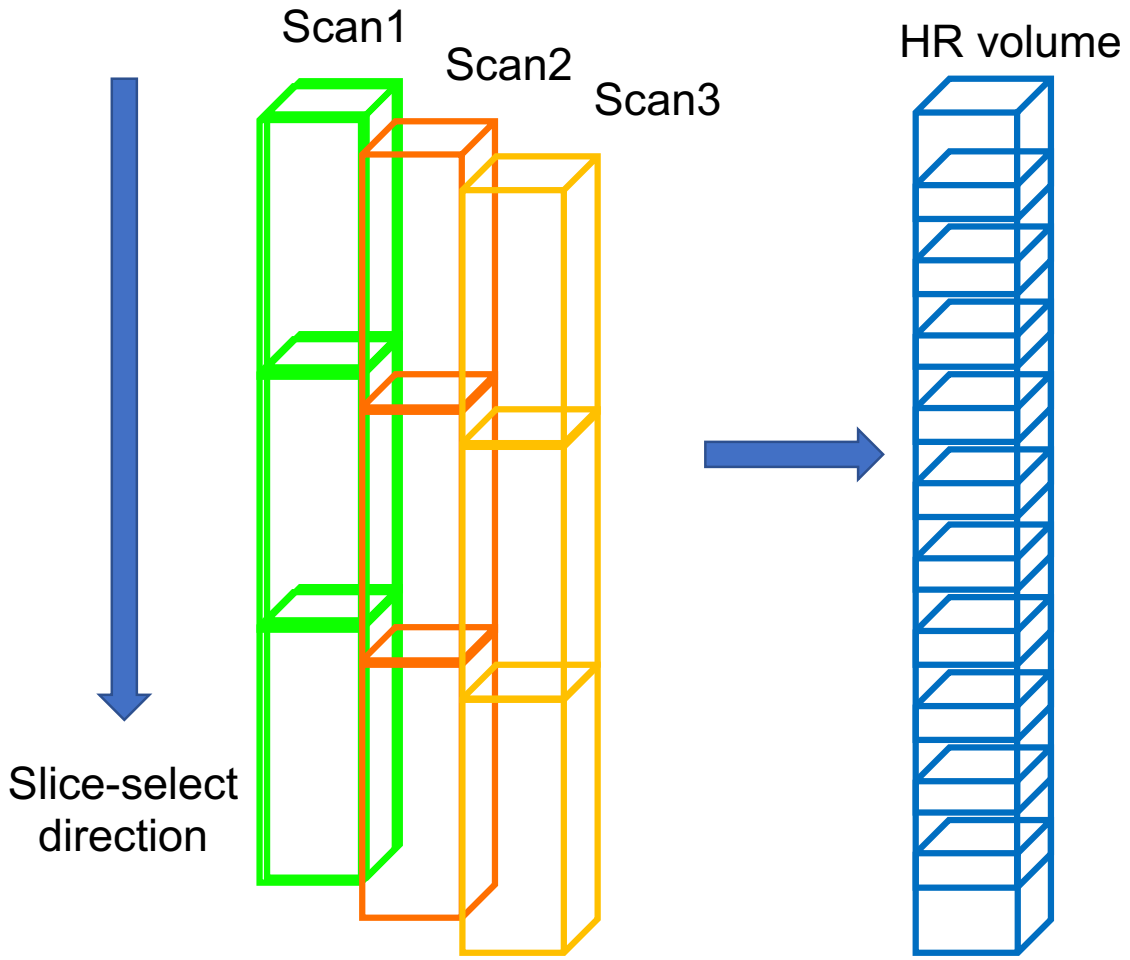

Fig. 1.3 MRI Reconstruction on SRR.

1.3.2 Single Image Super Resolution

With the introduction of single image super-resolution (SISR), MRI super-resolution reconstruction only requires a low-resolution scan corresponding to a high-resolution output. However, there are still problems, such as complex calculations.

The subsequent development of deep learning has led researchers to combine deep learning to perform MRI super-resolution reconstruction[13][14]. It uses a large number of high-resolution images to construct a learning library to generate a learning model(Figure 1.4). Restoring low-resolution images introduces the prior knowledge obtained by the learning model to obtain high-frequency details of the image and finally

obtain a better reconstruction effect[15]. The model SRCNN [16]based on CNN (Convolutional Neural Network) first introduced CNN into SISR. It only uses a three-layer network and uses PSNR, SSIM, and other evaluation standard algorithms to achieve advanced results. Subsequently, MRI super-resolution research began to try to combine convolutional neural networks for super-resolution reconstruction. With the introduction of residual learning[17], the super-resolution reconstruction network began to move in a deeper direction. At present, the SR reconstruction algorithm based on CNN has been developed rapidly. New network structures and training strategies have continuously improved the quality of SR reconstructed images, but these algorithms tend to output too smooth results without sufficient high-frequency details. Furthermore, the measurement results based on PSNR are inconsistent with human subjective evaluation. This problem began to be solved with Goodfellow's[18] proposal. SISR began to develop to improve the overall visual effect of the reconstructed image. Later, MRI's super-resolution reconstruction work focused on GAN to restore more texture details and high-frequency information rather than overall clarity.

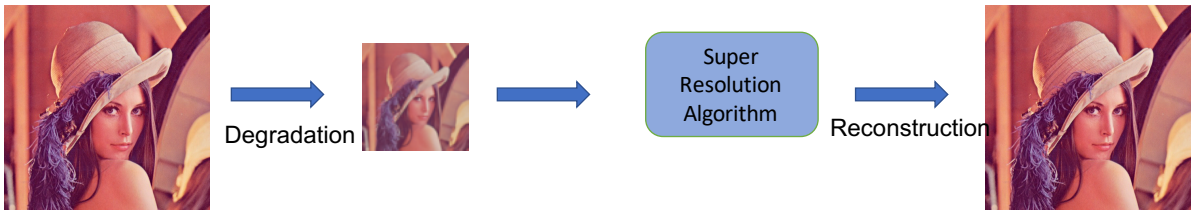

Fig. 1.4 Super Resolution in deep learning.

1.4 Main Contribution

The contributions of this paper mainly include the following three points:

1. We propose a two-dimensional MRI-based three-dimensional reconstruction method through two super-resolution generative adversarial networks.

2. The RAMA-GAN combined with the residual multi-scale module attention mechanism is proposed to recover the high-frequency details of MRI. At the same time, we also propose a new network(nESRGAN) for MRI image restoration. The noise added part of nESRGAN could provide certain high-frequency information and details without affecting the overall feature restoration. At the same time, the interpolation part of the up-sampling part can solve the artifact problem caused by the checkerboard effect. The network's global residual module and branch sampling module reduce the loss of detail caused by upsampling.

3. The method we proposed has achieved good performance in visual effects and high-frequency details. The obtained high-resolution MRI can help doctors get more brain information, which is particularly important for diagnosing and predicting brain diseases.

Chapter 2

Proposed methods and reconstruction

This chapter mainly introduces the main reconstruction steps in the research and the neural network used.

2.1 Main Idea and Processes

2.1.1 MRI and 2D Reconstruction

In MRI, evenly spaced 2D slice views generated by acquisition equipment are usually stacked on top of each other into a three-dimensional volume. From this 3D volume, we can obtain slices in any direction. The stacking method is shown in the figure 2.1.

Traditionally, MRI provides views in three main orthogonal directions, mainly axial, sagittal, and coronal. As shown in the figure 2.2, three slices in orthogonal directions are stacked to form the MRI volume. MRI is usually saved in a three-dimensional pixel matrix, and slice information is saved in three dimensions.

A three-dimensional convolutional neural network is generally used for super-resolution reconstruction in the traditional MRI super-resolution reconstruction technology. However, considering the memory limitations of the real GPU, it is more difficult to reconstruct the entire MRI at once. Therefore, in the three-dimensional convolutional neural network, the MRI is divided into blocks and reconstructed, and

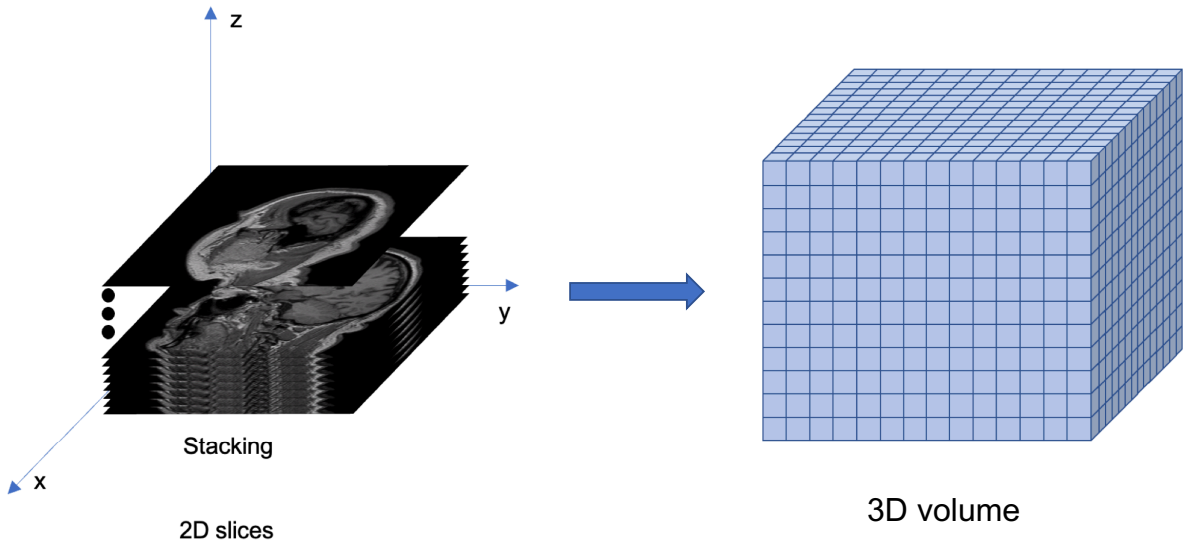

Fig. 2.1 MRI 2D slices and 3D volume.

then perform the block combination[19]. As shown in the 3DCNN steps in the figure 2.3, this method not only has an enormous time cost but also has the problem of memory limitation. Our research is based on MRI slices through two-dimensional slices to carry out MRI reconstruction, reducing training costs and memory allocation problems. Considering the characteristics of the 3D pixel matrix of MRI, by traversing the three dimensions of MRI, we can obtain slices in three orthogonal directions. We set a scale factor of 2 in the experiment. Combined with the matrix characteristics of MRI, obtaining the entire MRI requires half the number of slices to be prepared as the recombination condition, as shown in the 2DCNN step in the figure 2.3. Moreover, based on the particularity of MRI, although the number of reconstructed slices is only half in the three dimensions, MRI can still be reconstructed. There are many noises and missing values in the reconstructed MRI, as shown in figure 2.4. The insufficient number of slices causes this problem. In the beginning, we consider that the reconstructed slice has much high-frequency information, which can be interpolated and repaired by surrounding pixel values[20]. However, interpolation repair will only

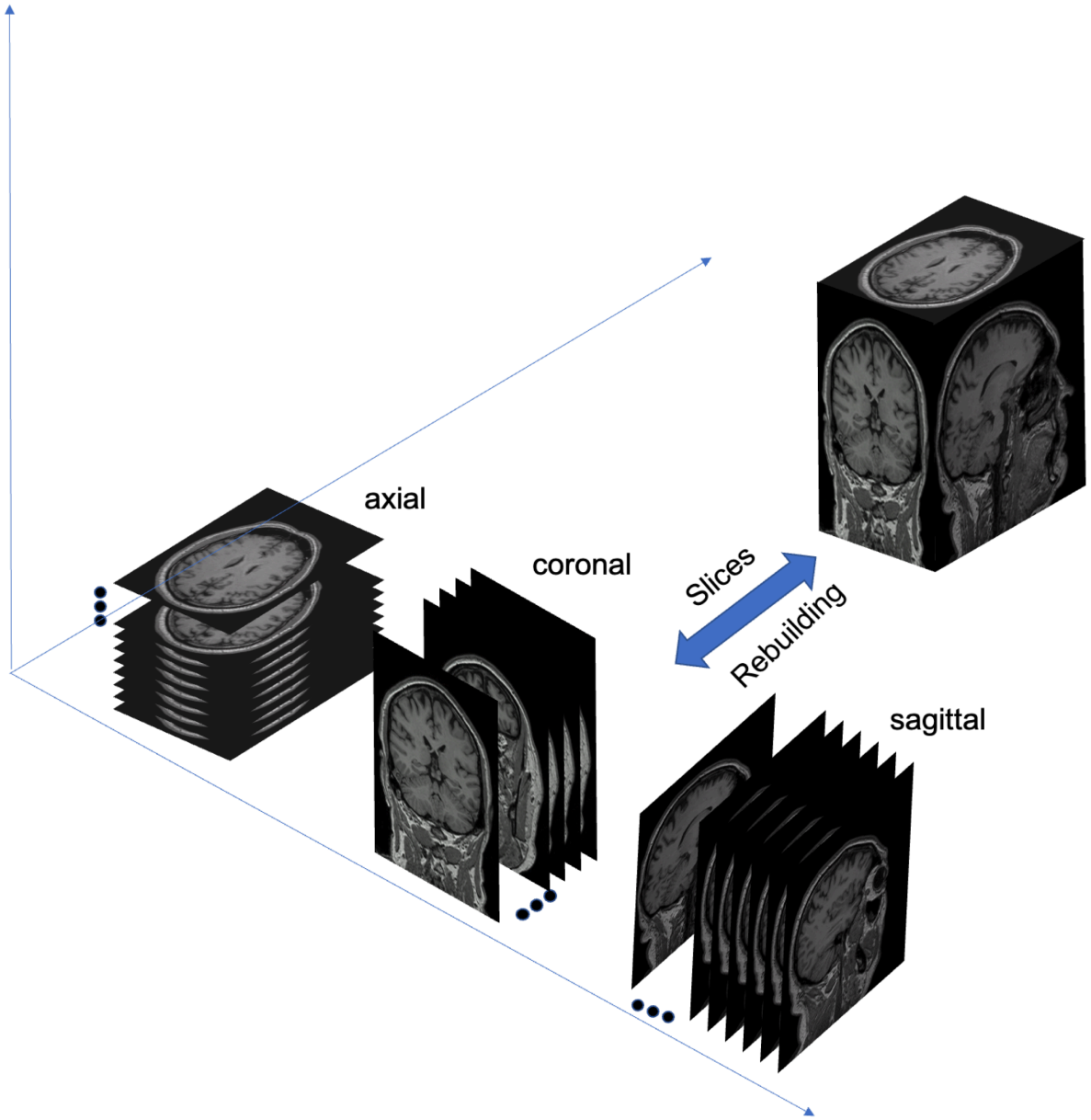

Fig. 2.2 MRI Rebuilding with three plane slices.

restore more low-frequency information and enlarge the influence of the noise part and the missing value part, resulting in more blurred areas. Therefore, we set up a second network to perform a second super-resolution reconstruction of the entire MRI to restore the overall high-frequency information and details.

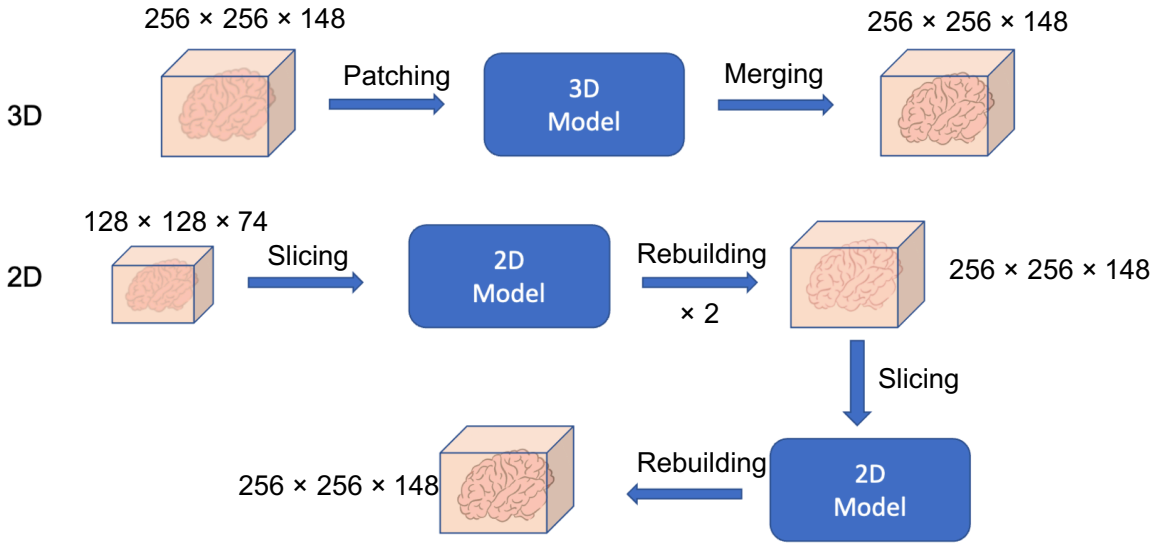

Fig. 2.3 MRI Reconstruction on 2D and 3D.

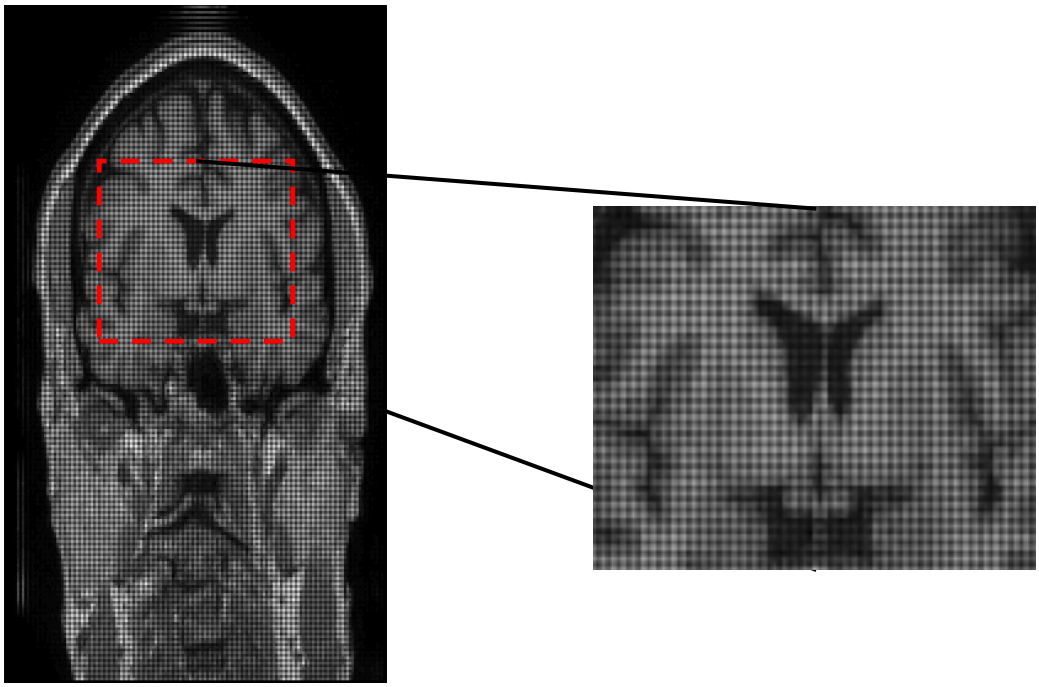

Fig. 2.4 The missing value and noise in MRI slice.

We take the new slice as a low-resolution image and then perform the super-

resolution reconstruction of the new network. Finally, we recombine the reconstructed MRI slice for the second time to obtain a high-resolution MRI. Figure 2.3 shows the comparison between 3D and 2D.

2.1.2 Processes

In the first reconstruction step, we propose two two-dimensional convolutional neural networks for three-dimensional reconstruction. We propose RMAM-GAN as a super-resolution reconstruction network. According to the parameter requirements, half of the slices are reconstructed in the first MRI reconstruction. The reconstructed MRI has only half of the slices in all three dimensions. Every slice has missing values in this new MRI, so we propose a noise-based network nESRGAN for the second super-resolution reconstruction. Inspired by StyleGAN[21], we find that adding noise can help restore features to a certain extent and supplement more high-frequency information.

Similarly, ESRGAN has the problem of the checkerboard effect caused by deconvolution[22]. For this reason, we propose a new interpolation sampling recovery block to replace the deconvolution layer so that the reconstructed image no longer has artifacts. Besides, the setting of the global residual module reduces the loss of detail caused by sampling.

In general, we adopt RMAM-GAN as the first MRI reconstruction method. Then half of the MRI slices are reorganized to obtain an MRI with a lot of noise and missing values. Next, we utilize nESRGAN to perform the second reconstruction. Traverse all the slices of the new MRI, and then use nESRGAN for super-resolution reconstruction, and finally rebuild a new high-resolution MRI. The main processes are shown in figure 2.5.

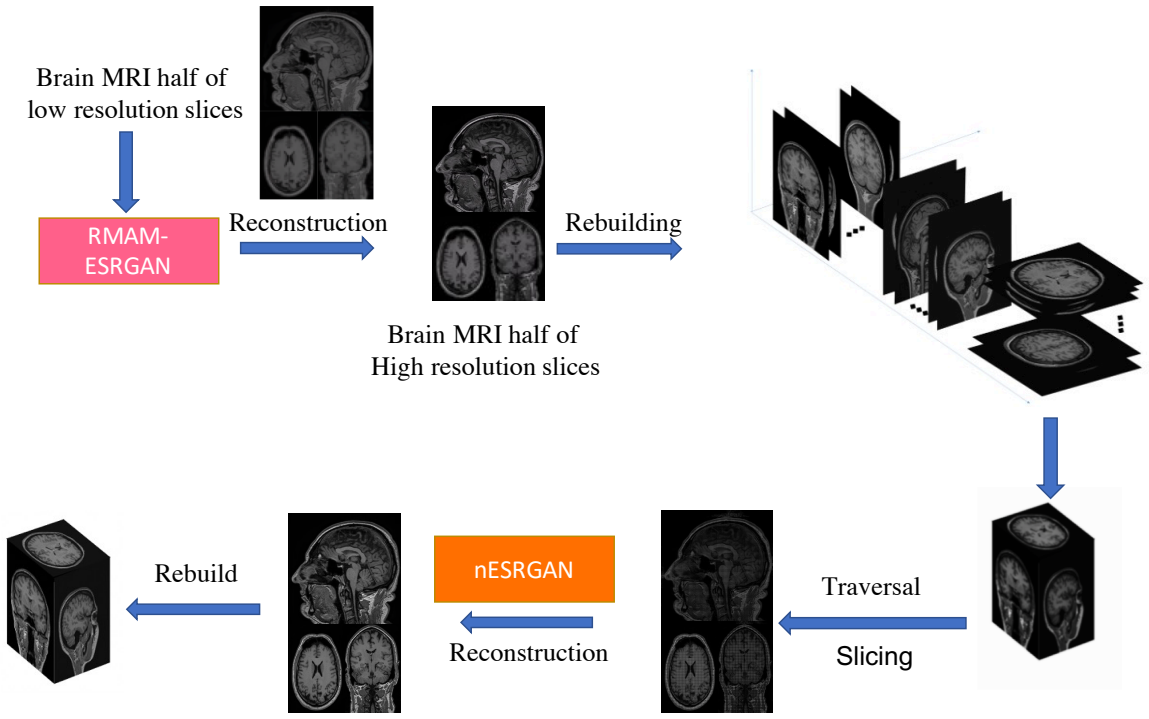

Fig. 2.5 The main processes in this research.

2.2 First MRI Slice Reconstruction

2.2.1 RMAM-GAN

Our previous first reconstruction work was to use GAN with perceptual domain blocks for MRI super-resolution reconstruction[23][24]. Considering the possibility of multi-scale reconstruction in the future and the starting point of focusing on more information features, we adopt the residual multi-scale module with an attention mechanism module[25] to replace RFB to obtain more feature information. The network is built based on the framework of ESRGAN, which includes two main modules, as shown in block A and block B in figure 2.6. Among them, block A represents Residual in Residual Dense block[26][27]. This setting can increase not only the depth of the network but also realize a more complex structure. The network can learn finer details. Block B is Dense bLock with RMAM, which is mainly used to extract detailed features. The

up-sampling part of the network uses a combination of interpolation and up-sampling to achieve a good blend of spatial information and depth information and reduce the

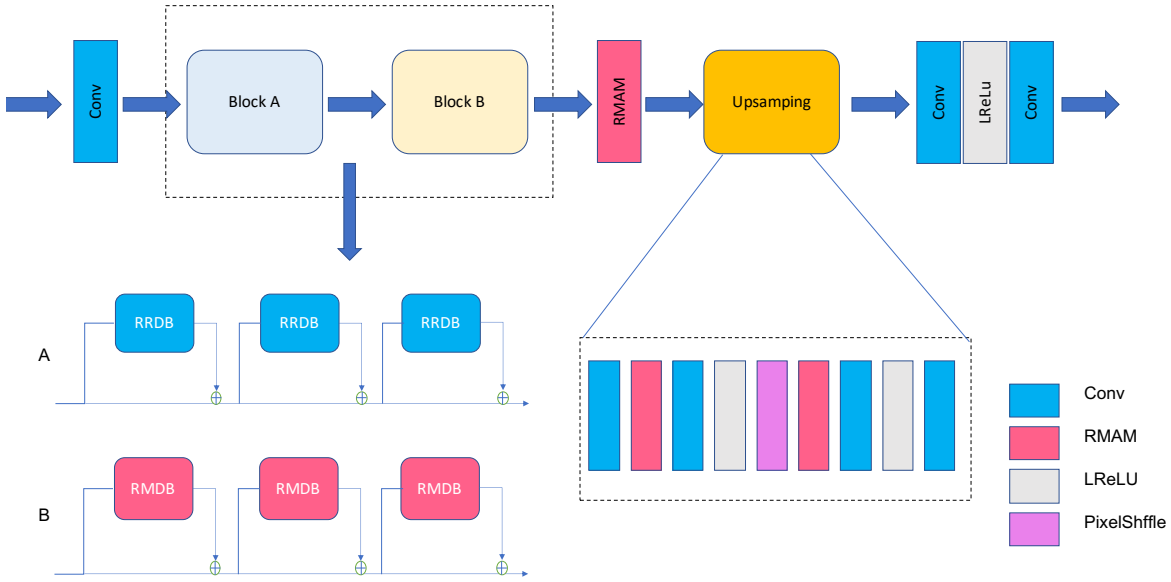

Fig. 2.6 The structure of RMAM-GAN.

loss of detail performance. Through RMAM-GAN, high-resolution MRI slices with rich, detailed information can be obtained.

2.2.2 RRDB

In previous studies, deep neural networks are difficult to train, and the gradient dispersion and explosion problem make it difficult for model training to converge. Although this problem has primarily been effectively controlled by standard initialization and intermediate layer normalization methods, these methods allow deep neural networks to converge. On the premise that the neural network can converge, as the network's depth increases, the network's performance first gradually increases to saturation and then decreases rapidly. With the introduction of the residual network, gradient disappearance and gradient explosion have been solved, allowing us to train a deeper network while ensuring good performance. As shown in figure 2.7, the residual blocks are stacked

together to form an intense neural network. Later, the deep network DenseNet[28] was proposed to directly connect all layers to ensure maximum information transmission between layers in the network. This method alleviates the problem of gradient disappearance and also strengthens the transmission and utilization of features. To a certain extent, the number of parameters is reduced. The RRDB in RMAM-GAN combines deep network and residual network, which can ensure smaller parameters while improving feature extraction capabilities. The main structure of the network is shown in Figure 2.8.

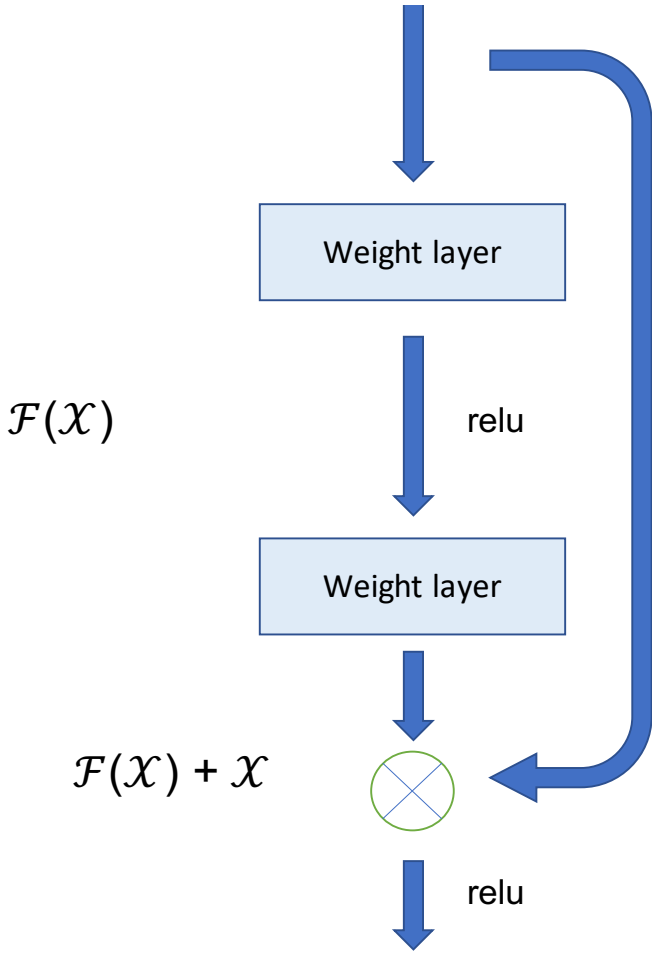

Fig. 2.7 The idea of residual net.

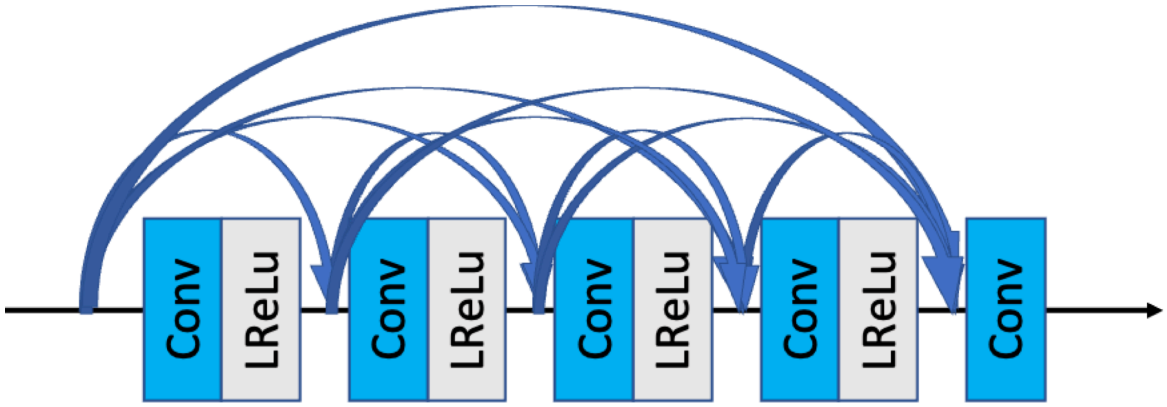

Fig. 2.8 RRDB.

2.2.3 RMAM

Similarly, the RMDB in RMAM-GAN also adopts the same structure, using the RMAM module in the network structure, as shown in figure 2.9. RMAM is a multi-

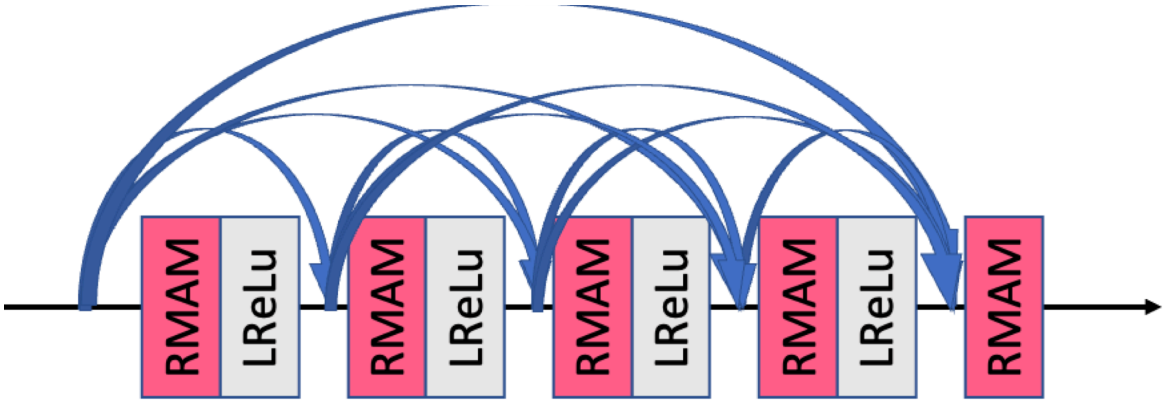

Fig. 2.9 RMDB

feature fusion module that combines multiple small convolution kernels. The 1x1 convolution in the module has two advantages. On the one hand, the filter is small, and the calculation is fast. On the other hand, it can improve the non-linearity of the network to learn more complicated mapping relationships. The module uses small filters to reduce parameters and calculations and uses a more extensive range of receptive fields to transmit information after acquiring features. The features of multiple channels are merged,

and SEnet[29] is used to enhance the sensitivity of the model to channel features. By weighting the channels, effective information is emphasized, and invalid information is suppressed. Moreover, it adjusts the relationship between channels to make their weights more reasonable, thereby improving the SR performance of the network. The structure of the module is shown in figure 2.10. In general, the RMAM module

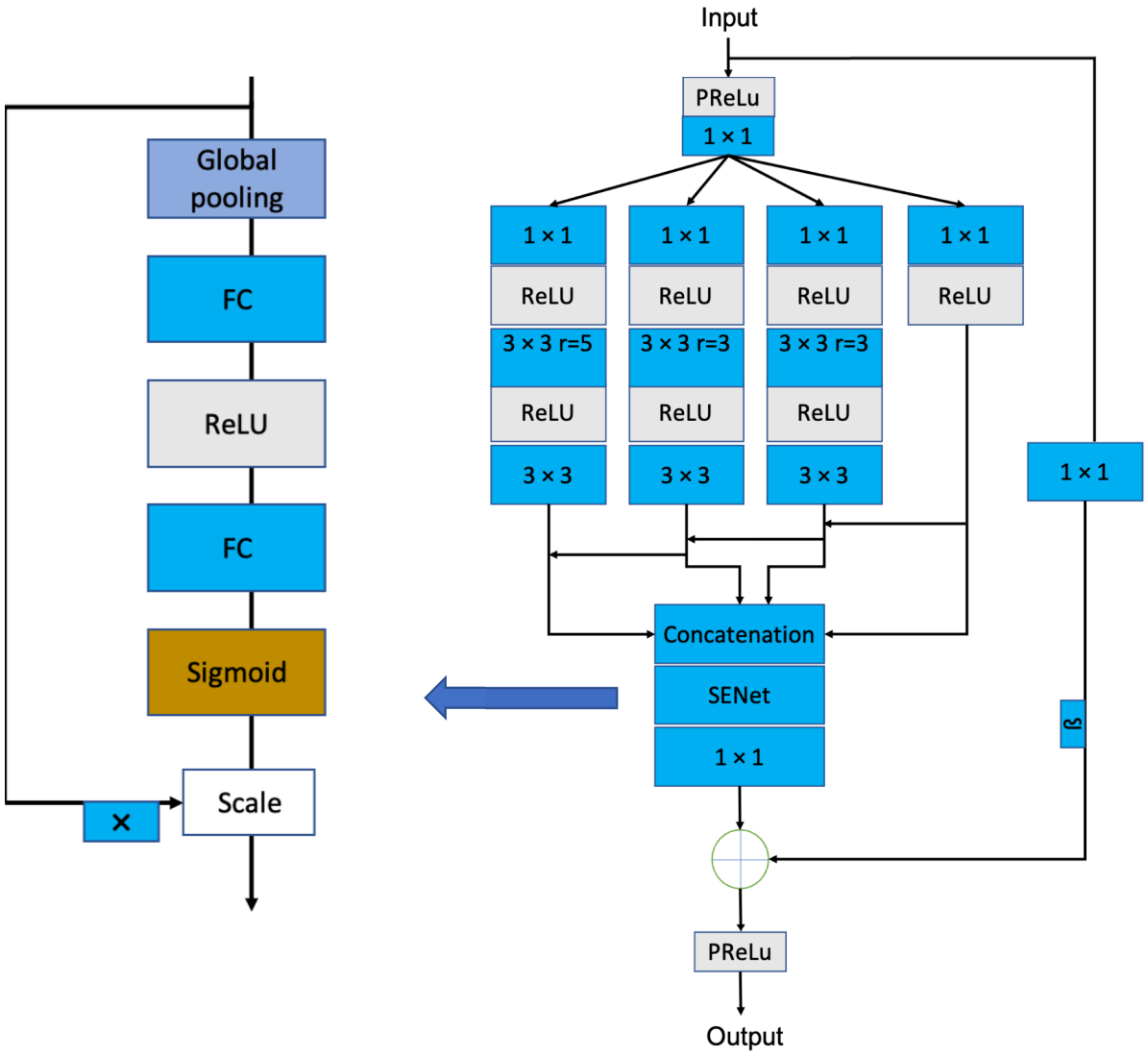

Fig. 2.10 The structure of RMAM.

strengthens the interactivity of each channel, and this setting can extract very detailed features.

2.2.4 Upsampling

The up-sampling part of the network consists of the RMAM module and nearest-neighbor interpolation and Sub-pixel Convolution (SPC) alternately. Nearest Neighborhood Interpolation (NNI) plays a role in the spatial conversion of input features and then connects to the RMAM layer to diffuse its spatial influence in depth. SPC performs a depth-to-space transformation and then connects to the RMAM layer to enhance the transformation within the spatial range. The specific structure is shown in figure 2.6.

2.2.5 Patch Discriminator

The discriminators of the previous super-resolution generative adversarial network all adopt the VGG128 structure[30]. The main structure of the discriminator is shown in figure 2.11. The discriminator network pays more attention to the overall image features rather than the local image features. That is to say, this structure usually only needs to output a scalar, which is used to distinguish two categories. Therefore, we adopt the structure of Patch Discriminator[31] on the discriminator. The output of PatchGAN is a two-dimensional matrix. Each value represents the judgment of the local area of the image so that the local texture details of the image can be paid attention to and enhanced. In addition, we use a relativistic discriminator[32] as the loss criterion.

The relativistic discriminator could provide the probability that one image is more accurate than another image. This method can make the generator generate more realistic texture details.

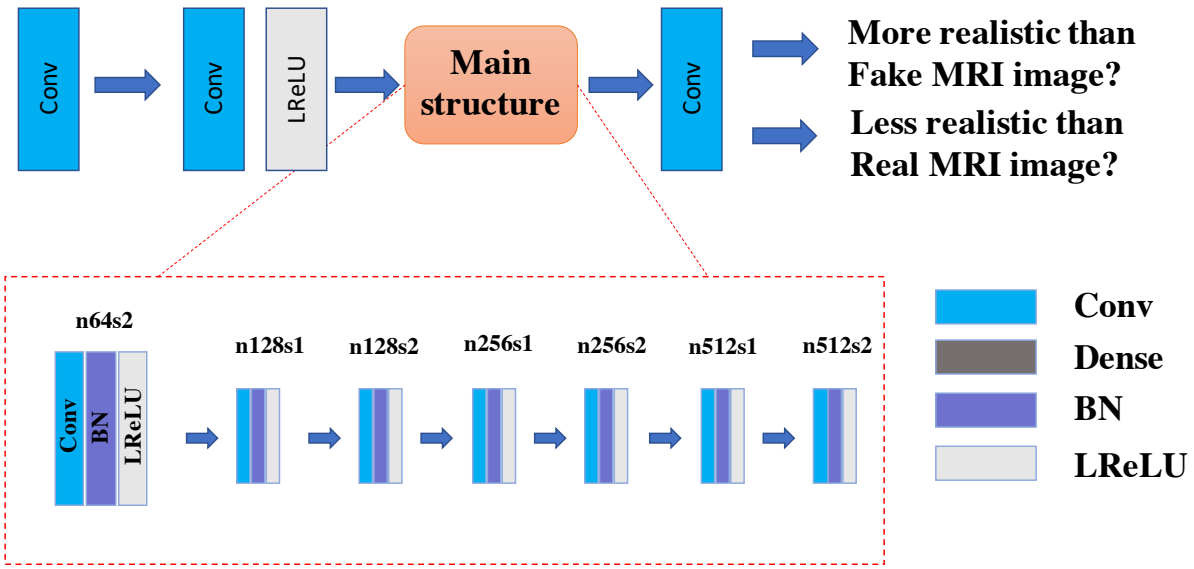

Fig. 2.11 The network of discriminator.

2.3 Second MRI Slice Reconstruction

2.3.1 nESRGAN

After completing the first MRI super-resolution reconstruction, combined with the problems that occurred after the recombination mentioned, we hope to maintain a better reconstruction performance as much as possible while ensuring a small amount of calculation. We propose a new super-resolution network, nESRGAN, as the network for the second super-resolution reconstruction. We perform the second slice processing on the reorganized MRI, and the obtained MRI slice is used as a new dataset. Considering the noise and missing areas of the slice, we regard the dataset as a low-resolution image that has undergone image degradation. The main architecture of the network is shown in figure 2.12. The network is based on ESRGAN, mainly composed of a noise-adding module, an up-sampling module, and a global residual module. The discriminator part is consistent with RMAM-GAN. nESRGAN can recover detailed information, and the overall network complexity is not enormous, which is suitable for the rapid progress of

the second reconstruction work.

2.3.2 noise

Based on the problem of missing values, inspired by StyleGAN's added noise[21] to achieve the diversity of details, we add random Gaussian noise to RRDB. This kind of noise is added to the residual dense block residual, which can generate certain detailed information. The noise part in Figure 2.12 shows the central architecture.

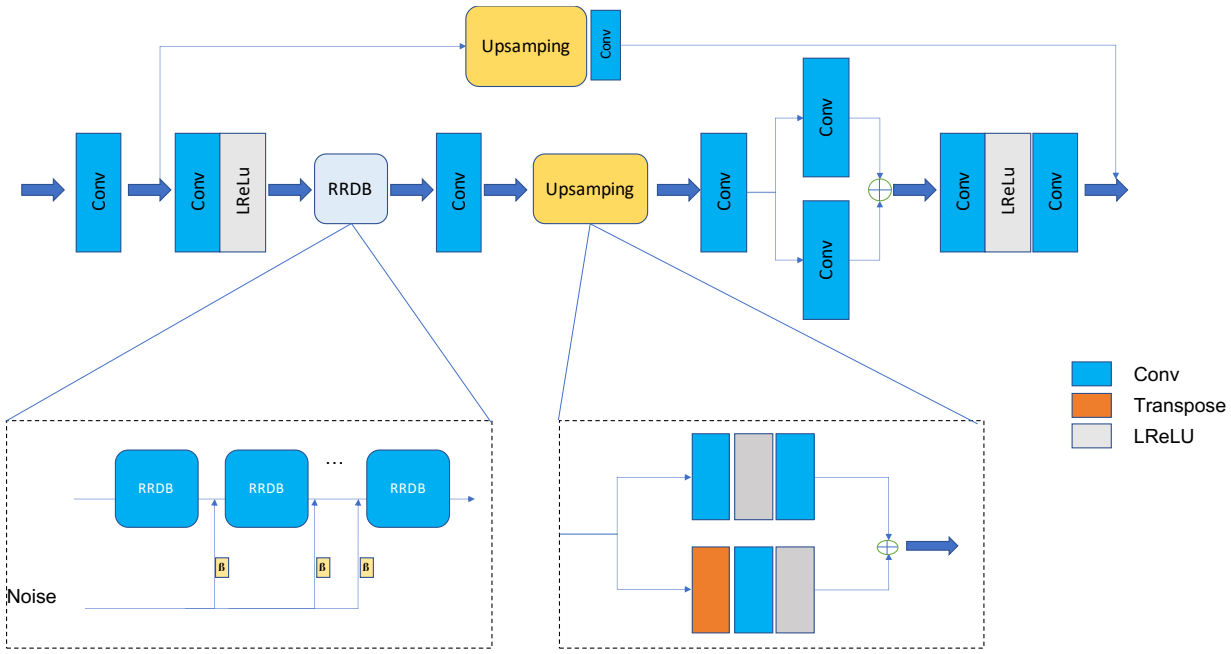

Fig. 2.12 The structure of nESRGAN.

2.3.3 Global Residual Block

In the super-resolution reconstruction process, we set up two branches for upsampling. Using the fusion of the two branches of interpolation sampling and deconvolution can avoid the checkerboard effect happens. In addition, the up-sampling step usually results in the loss of information. For this reason, we set up a branch convolution fusion after upsampling to reduce the loss of information. In addition, inspired by U-net's[33]

global context information, we set up a global residual module in the network. The global residual module merges the feature information of the input image with the output image. This setting also reduces the loss of feature information and improves the SISR performance.

2.4 Related Loss Function

2.4.1 Generator loss

The loss functions of the two networks in the reconstruction process are consistent. The generator network loss is mainly composed of content loss, perceptual loss, and confront loss[34]. Content loss refers to the L1 of the supervised learning enhancement output and label, which calculates the pixel loss between the predicted image and the target image. The content loss can be expressed as follows:

$$l_1 = -E[log(1 - \Delta_{Real})] - E[log(\Delta_{Fake})] \tag{2.1}$$

$$\Delta_{Real} = sigmoid(D(I^{HR}) - E[D(I^{SR}]) \tag{2.2}$$

$$\Delta_{Fake} = sigmoid(D(I^{SR}) - E[D(I^{HR}]) \tag{2.3}$$

$$L_{cont} = \eta l_1 \tag{2.4}$$

The perceptual loss compares the high-level perception and semantic differences between images. The low-level feature information of the image is extracted through the VGG19 network before activation. These low-level feature tensors can be compared through simple pixel-level loss. The perceptual loss can be expressed as follows:

$$I^{SR} = G(I^{LR}) \tag{2.5}$$

$$L_{percep} = \Sigma||VGG(I^{SR}) - VGG(I^{HR})||_1 \tag{2.6}$$

In addition, the generator loss refers to the loss when confronting the discriminator, which is mainly expressed as follows:

$$L_G^{Ra} = \Sigma||I^{SR} - I^{HR}||_1 \tag{2.7}$$

$$L_G^D = \lambda L_G^{Ra} \tag{2.8}$$

In general, the generator loss can be represented by:

$$L_G = L_{percep} + \lambda L_G^{Ra} + \eta l_1 \tag{2.9}$$

On the whole, the perceptual loss is extracted from the image features through the VGG19 network, and the features obtained from the real image convolution are compared with the features obtained from the generated image convolution, so that the high-level information (content and global structure) is close. $VGG(I^{SR})$ and $VGG(I^{HR})$ are real MRI image and generated MRI image, respectively. L_G^{Ra} reflects the probability of generating a more realistic slice. Both λ and η are coefficients that balance different loss terms.

2.4.2 Adversarial loss

The idea of RaGAN is adopted in the discriminator network, mainly to calculate the probability that the real image is relatively more realistic than the fake image. The discriminator loss can be expressed as follows:

$$L_D = -E[log(\Delta_{Real})] - E[log(1 - \Delta_{Fake})] \tag{2.10}$$

2.5 Image Quality Evaluation Indicators

2.5.1 PSNR and SSIM

In the super-resolution algorithm, the image quality of the super-resolution picture will be evaluated after the reconstruction work is completed. It is more common to use PSNR and SSIM[35]as evaluation criteria. Considering that PSNR and SSIM often have evaluations that do not meet the actual human visual effects, we have added LPIPS to the experiment for image evaluation. PSNR (Peak Signal to Noise Ratio) is the most common and widely used objective standard for evaluating images. In order to measure the image quality after processing, we usually refer to the PSNR value to measure whether a specific processing program can be satisfactory. However, many experimental results show that it has limitations. The PSNR score cannot be the same as the visual quality seen by the human eyes. The higher PSNR may look worse than the lower PSNR. PSNR is mainly represented by:

$$PSNR = 10 \times log_{10} \frac{MAX_I^2}{MSE} \tag{2.11}$$

Among them, MSE represents the mean square error (Mean Square Error) of the current image X and the reference image Y, and H and W are the height and width of the image, respectively. The main expressions are as follows:

$$MSE = \frac{1}{HW} \sum_{i=1}^{H} \sum_{j=1}^{W} [X(i,j) - Y(i,j)]^2 \tag{2.12}$$

SSIM (structural similarity) is also a full-reference image quality evaluation index, which measures image similarity from three aspects: brightness, contrast, and structure. The main formula is as follows:

$$SSIM(x,y) = \frac{(2\mu_x\mu_y + c_1)(2\sigma_{xy} + c_2)}{(\mu_x^2 + \mu_y^2 + c_1)(\sigma_x^2 + \sigma_y^2 + c_2)} \tag{2.13}$$

μ_x and μ_y represent the average of images X and Y, σ_{xy} represents the covariance of images X and Y, and σ_x and σ_y represent the variance of images X and Y. The value range of SSIM is [0,1]. Generally speaking, the larger the SSIM value, the smaller the image distortion.

2.5.2 LPIPS

The unreasonable effectiveness of deep features as a perceptual metric-LPIPS[36] is a perceptual similarity measure based on learning. Perceiving similarity is not a particular function in itself but the result of visual representations that predict essential structures in the world. Although PSNR and SSIM are widely used, they often fail to provide feedback that meets natural sensory conditions. Therefore, we also add LPIPS as the image quality evaluation standard in the evaluation. The primary expressions are as follows:

$$d\left(x, x_0\right)=\sum_l \frac{1}{H_l W_l} \sum_{h, w}\left\|w_l \odot\left(\hat{y}_{h w}^l-\hat{y}_{0 h w}^l\right)\right\|_2^2 \tag{2.14}$$

Among them, d is the distance between x_0 and x. The feature stack is extracted from the L layer and unit-normalized in the channel dimension. Use the vector $w_l = R^{C_l}$ to scale the number of activated channels and calculate the L2 distance, average in space, and sum on the channel.

Chapter 3

Configuration and Comparison

This chapter mainly introduces the experiment's configuration, including the experimental environment, dataset, and experimental configuration. In addition, we also show the comparison of some parameter settings on the two networks.

3.1 Experimental Configuration

3.1.1 Experimental Environment

Our super-resolution reconstruction network is based on PyTorch. Torch is a classic tensor library that operates on multi-dimensional matrix data. It is widely used in machine learning and other math-intensive applications. Pytorch is the python version of the torch and a neural network framework open-sourced by Facebook. In the entire network, we use GPU for network training. The specific configuration information is shown in Table 3.1:

Table 3.1 Experimental Configuration.

CPU-model :	Intel(R) Xeon(R) CPU E5-2698 v4 @ 2.20GHz
Graphics ：	Tesla V100-SXM2-32G
Operating System :	Ubuntu 16.04.10 LTS
Scripting language :	Python 3.6.10
Neural network framework:	Pytorch

3.1.2 Dataset

The data set in the experiment is mainly composed of IXI (Information eXtraction from Images) dataset[37], Kenshin dataset, and Simon dataset[38]. A total of 352 T1 brain MRI data sets were used in the experiment. The specific information of the data set is shown in the table 3.2:

Table 3.2 The information of MRI dataset.

Dataset	number	Manufacturer	Model
IXI	200	Philips system	T1
Kenshin	100	Hitachi-ECHELON	T1
Simon	52	Philips and Siemens	T1

In our previous work, bicubic interpolation was used as the image degradation processing method. However, the low-resolution MRI slices obtained often cannot meet the low-resolution conditions of the real world. Low-resolution MRI slices usually have problems such as noise and blur. Bicubic cannot achieve better performance in actual super-resolution reconstruction through simple interpolation degradation. In addition, it is not easy to use unsupervised learning to generate low-resolution MRI. Therefore, we adopt a new integrated standard medical image processing library Torchio[39] to perform MRI slice image degradation processing. Torchio is an open-source python data package responsible for the processing of medical images. It solves the problem of the lack of a large number of paired information medical image data sets in the real world. We performed four image degradation processing operations on the dataset, namely Gaussian blur, Gaussian noise, motion blur, and motion blur with Gaussian noise added[40][41]. The main preprocessing is shown as figure 3.1:

We select three slices on the Plane in the first super-resolution reconstruction work

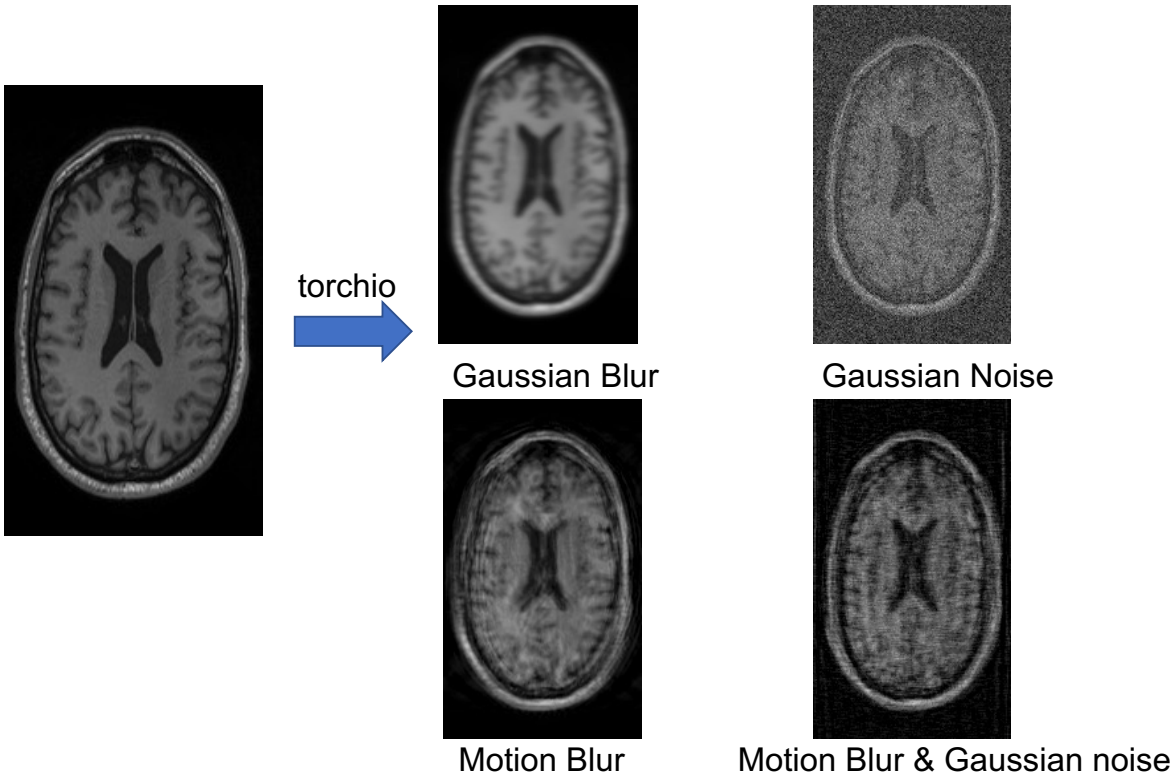

Fig. 3.1 The degenerative process of MRI. High-resolution MRI performs four kinds of degradation through Torchio: Gaussian blur, Gaussian noise, motion blur, motion blur, and Gaussian noise.

as the training set and the testing set. Table 3.3 and table 3.4 shows the information of the dataset for training and testing. In addition, we have performed data augmentation processing for the training set. The randomly selected slices are randomly cropped, and the size is 64 x 64. At the same time, the size of the pre-processed low-resolution slice is 32 x 32. After that, we perform half of the MRI slice reorganization, and the reorganization work adopted an interval of 1. After that, the MRI will be sliced and then randomly cropped. The size of HR-LR is also 64 x 64 and 32 x 32.

Table 3.3 RMAM-GAN

	Trainset	Testset
HR	64 x 64	64 x 64
LR	32 x 32	32 x 32
Numbers	62400	26750

Table 3.4 nESRGAN

	Trainset	Testset
HR	64 x 64	64 x 64
LR	32 x 32	32 x 32
Numbers	46700	20015

3.2 Comparison

3.2.1 RMAM-GAN

In the construction of RMAM-GAN, we compare the performance of reconstruction under different structures. As shown in figure 3.3, as the number of training increases, the overall performance of the RMAM module is great. In addition, figure 3.2 shows several different network architectures. The addition of the SEnet hardly affects the size of the parameters and improves the SR performance.

3.2.2 nESRGAN

In order to detect the status of each module in nESRGAN, we compare the three modules in a blending test. As shown in the table 3.5, in the evaluation of perceived similarity, the network with three modules performed best. In addition, combined with the noise module, the noise part can provide detailed information to a certain extent and improve the visual effect.

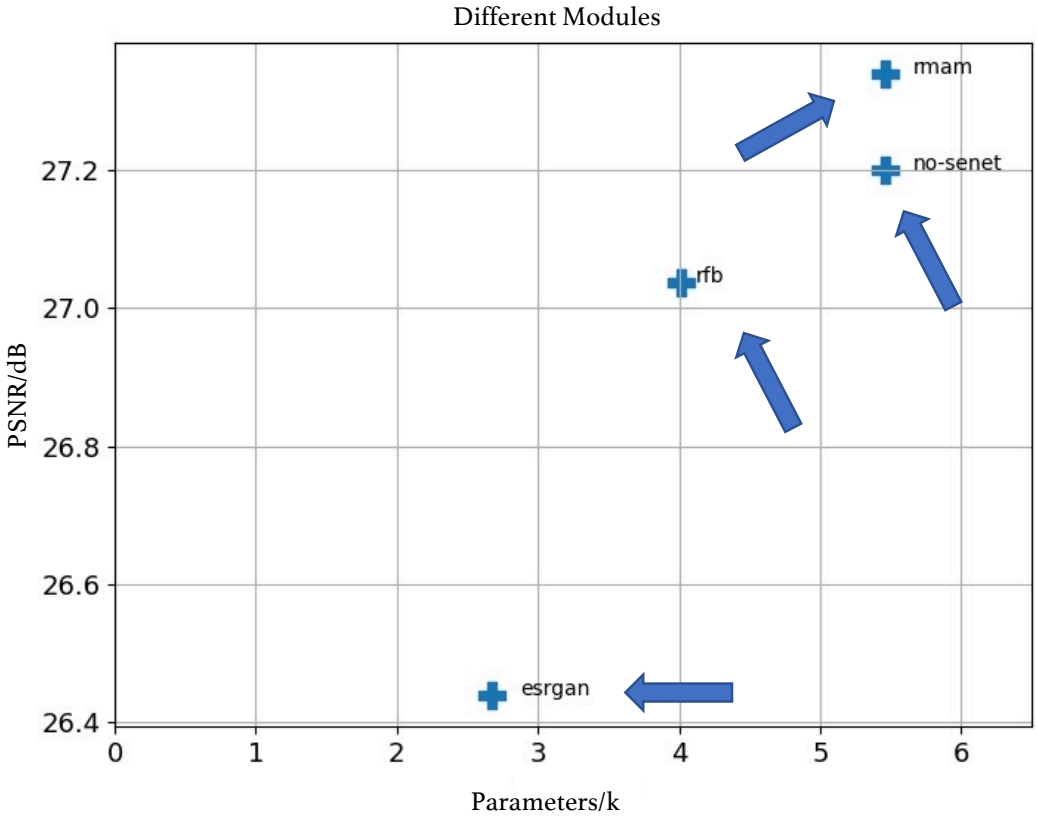

Fig. 3.2 Different module of second MRI Super Reconstruction.

Table 3.5 Comparison of different module in nESRGAN(mean ± standard deviation).

Module				
Global residual	√		√	√
Upsampling	√	√		√
Noise	√	√	√	
LPIPS ↓	**0.1271 ± 0.0110**	0.1749 ± 0.0103	0.1584 ± 0.0117	0.1762 ± 0.0139

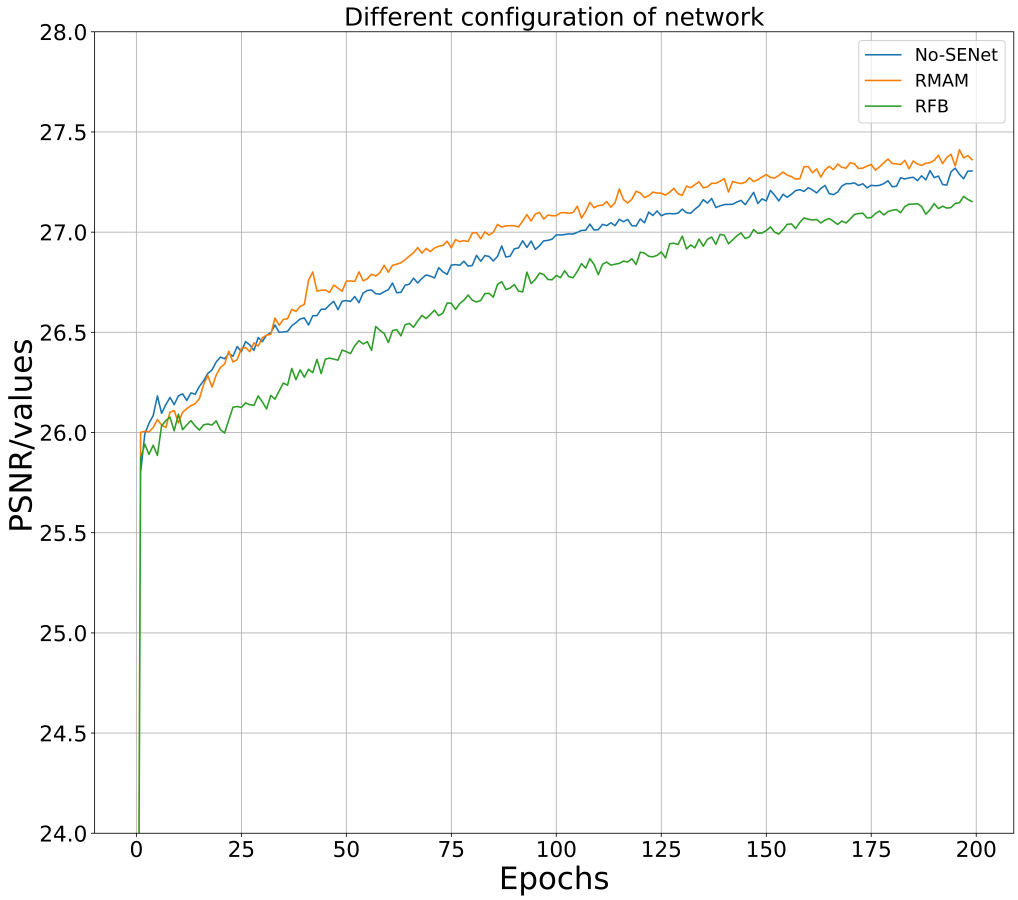

Fig. 3.3 The comparison of configuration on network.The PSNR of the three modules increases as the number of training increases. Comparing the three modules, RMAM performs best overall. Adding SEnet can indeed improve the reconstruction performance of the image.

Chapter 4

Result and Discussion

In this chapter, we mainly introduce and show the SR performance of the two reconstruction tasks. In addition, we also compare the reconstruction performance between 2D and 3D. Finally, we discussed the entire experiment.

4.1 First Super-Resolution Reconstruction

In order to verify the reconstruction performance of RMAM-GAN, we make a comparison during the first SR reconstruction process. As shown in table 4.1, we compare the traditional deep learning super-resolution network with RMAM-GAN. It can be seen from the table that RMAM-GAN performs best in image evaluation. In addition, in figure 4.1, we show the reconstructed slices under each network. It can be seen that the texture details also maintain superior performance.

4.2 Second Super-Resolution Reconstruction

After the first reconstruction using RFB-ESRGAN, we perform the second MRI reconstruction. The reconstructed MRI image is noisy and has missing values. We perform the second reconstruction of MRI through the proposed nESRGAN. In the second SR reconstruction work, we compare the pixel distribution and frequency domain to show the reconstruction situation more clearly. Figure 4.2 shows the image pixel distribution before and after reconstruction. The pixel distribution of the reconstructed

MRI image in the spatial domain is close to the original high resolution, indicating that the low-frequency components are similar. As shown in Figure 4.3, a is the MRI slice after the first reorganization, b and c are the reconstructed slice and the high-resolution GT-MRI, respectively. The peak point in the figure is the low-frequency component, and a has complex and irregular multiple low-frequency information. After nESRGAN super-resolution reconstruction, the distribution trend of b and c is the same. At the same time, the low-frequency information remains the same, which satisfies the convergence of the original GT image. There is a slight difference in the distribution of high-frequency components.

However, it is close to the original GT image.

We also compare and evaluate nESRGAN and standard super-resolution methods. As shown in table 4.2 and figure 4.4, although SRGAN performs best on PSNR, the feature details after reconstruction are insufficient. In general, nESRGAN performs better than other traditional networks in terms of visual hierarchy and image quality. After completing the second SR reconstruction, the high-resolution MRI is basically obtained. Our research has realized the replacement of 3D convolutional neural network reconstruction through two reconstructions on the 2D level.

Table 4.1 Comparison of different SR method in deep learning(mean ± standard deviation).

	PSNR(dB) ↑	SSIM ↑	LPIPS ↓
SRCNN	19.2607 ± 0.1361	0.5715 ± 0087	0.4275 ± 0086
FSRCNN	25.6614 ± 0.1527	0.8513 ± 0.0062	0.1989 ± 0.0075
EDSR	25.1103 ± 0.2437	0.8568 ± 0.0088	0.1789 ± 0.0080
SRGAN	25.5919 ± 0.1785	**0.8569 ± 0.0074**	0.1811 ± 0.0091
ESRGAN	25.1706 ± 0.1527	0.8360 ± 0.0070	0.1671 ± 0.0077
RRAM-GAN	**25.9050 ± 0.1765**	0.8517 ± 0.0078	**0.1642 ± 0.0105**

Table 4.2 Comparison of EDSR,SRGAN,ESRGAN,nESRGAN in second super resolution reconstruction step(mean ± standard deviation).

	PSNR(dB) ↑	SSIM ↑	LPIPS ↓
EDSR	26.7625 ± 0.3102	0.8604 ± 0.0143	0.1737 ± 0.0138
SRGAN	27.553 ± 0.4186	0.8234 ± 0.0112	0.1538 ± 0.0113
ESRGAN	27.2105 ± 0.2726	0.8585 ± 0.0029	0.1504 ± 0.0118
nESRGAN	**24.0622 ± 0.2212**	**0.8815 ± 0.0054**	**0.1242 ± 0.0063**

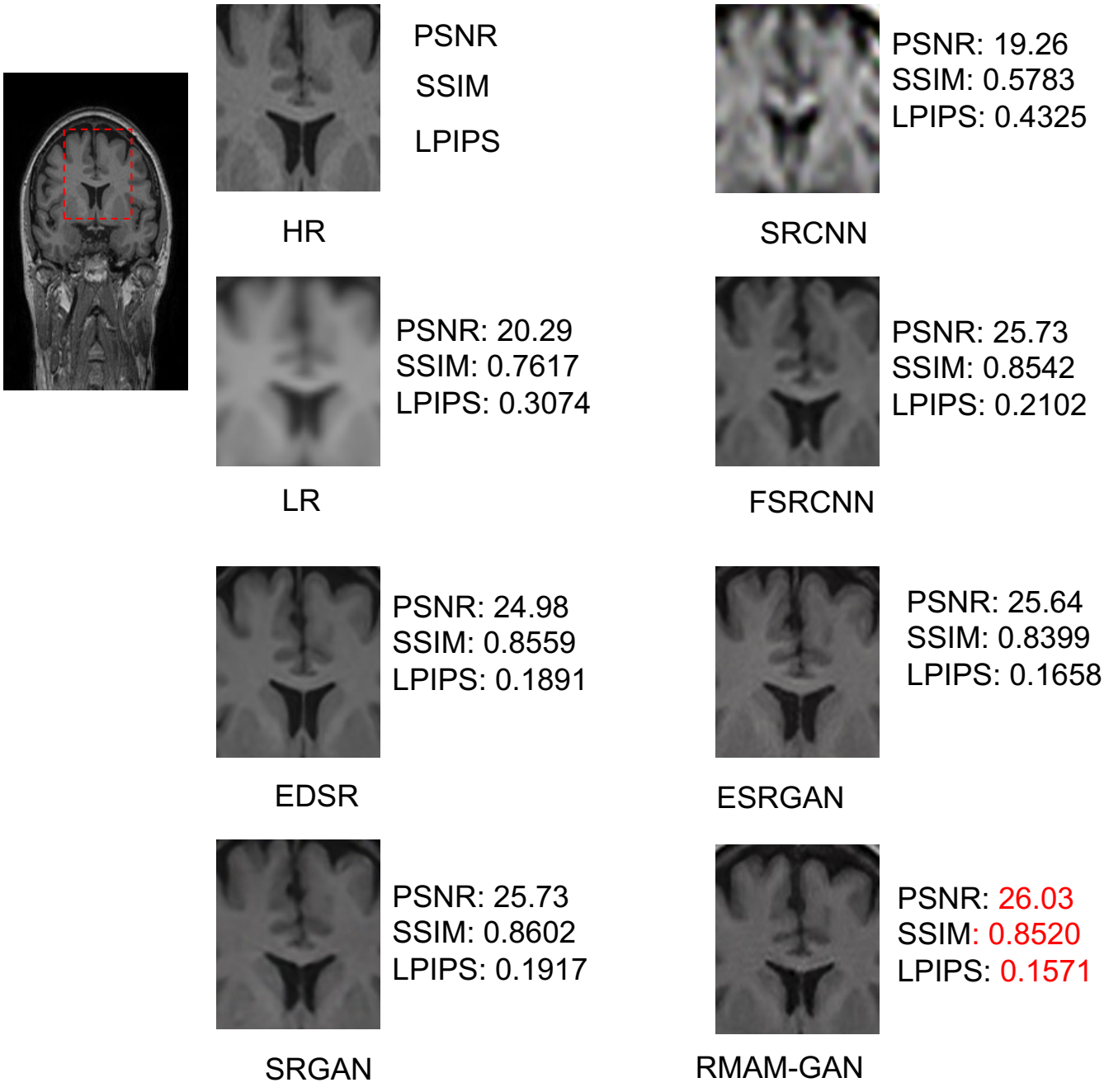

Fig. 4.1 Comparion of SRCNN,FSRCNN,EDSR,SRGAN,ESRGAN,and RMAM-GAN.

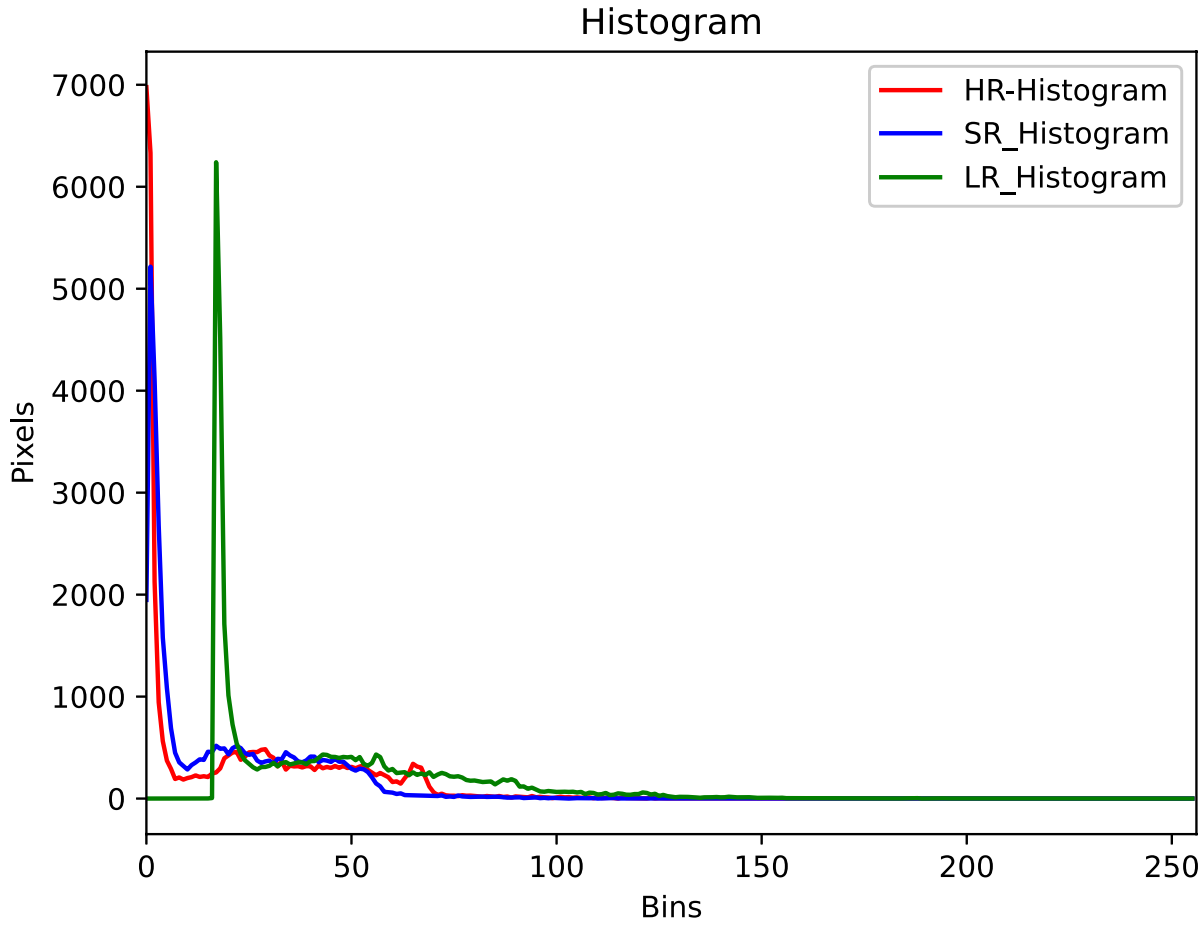

Fig. 4.2 The pixcel historgram of LR, SR and HR.

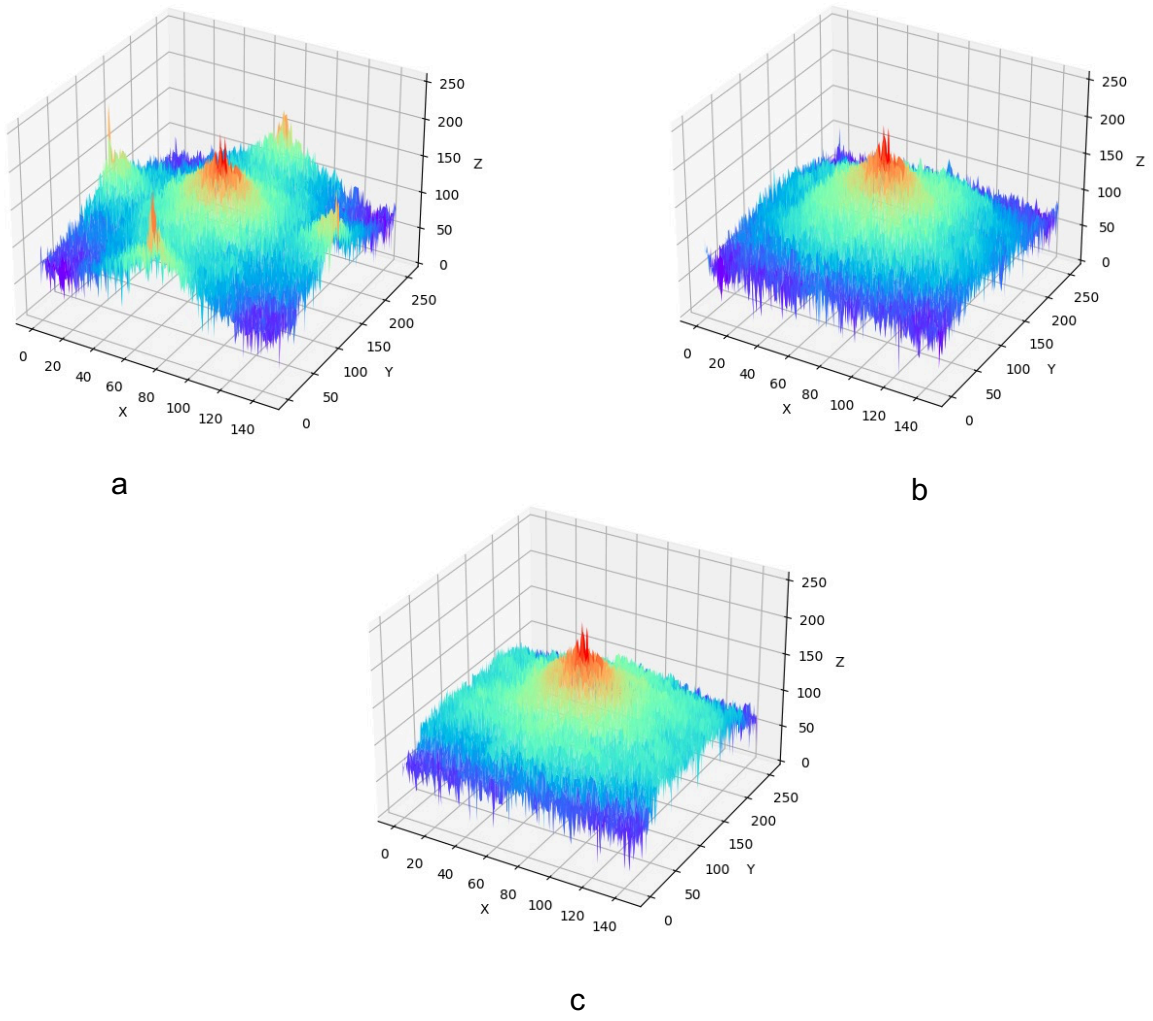

Fig. 4.3 Frequency distribution of LR,SR,HR.

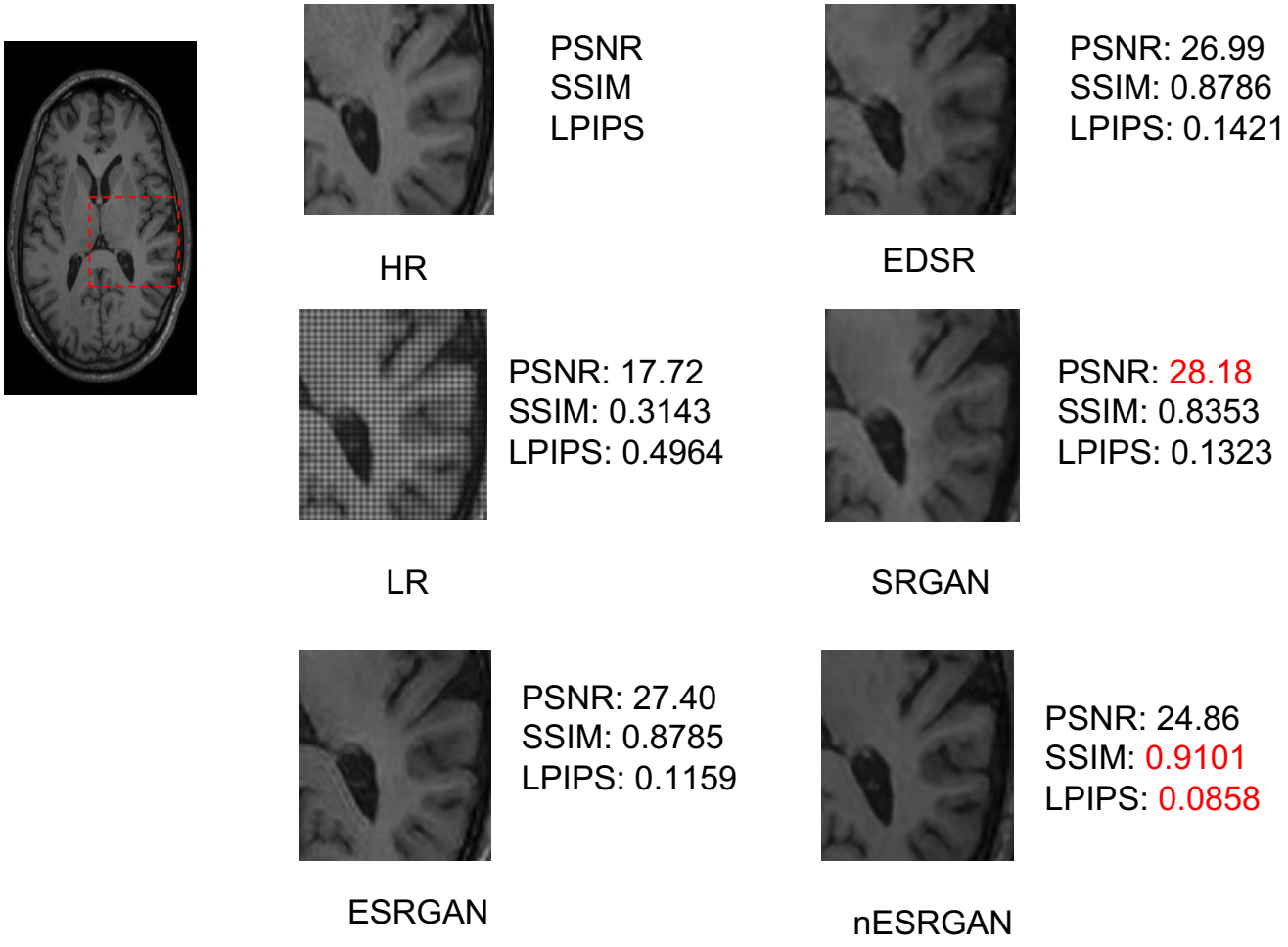

Fig. 4.4 Comparison of second reconstruction step.

4.3 2D vs 3D

Traditional MRI three-dimensional super-resolution reconstruction generally uses CNN or GAN to perform. We also compare our method with three-dimensional-based super-resolution methods. In figure 4.5 and figure 4.6, our method maintains a good advantage in PSNR and LPIPS. Besides, as shown in table 4.4, table 4.4 shows the comparison of the three datasets after reconstruction under each method. It can be seen from the table that our method maintains advantages in image evaluation compared to 3DSRCNN[42] and 3D-SRGAN[43]. In addition, from the figure 4.7, 3D-SRGAN and our method are better than other methods. In terms of texture details, our method is superior to 3D-SRGAN.

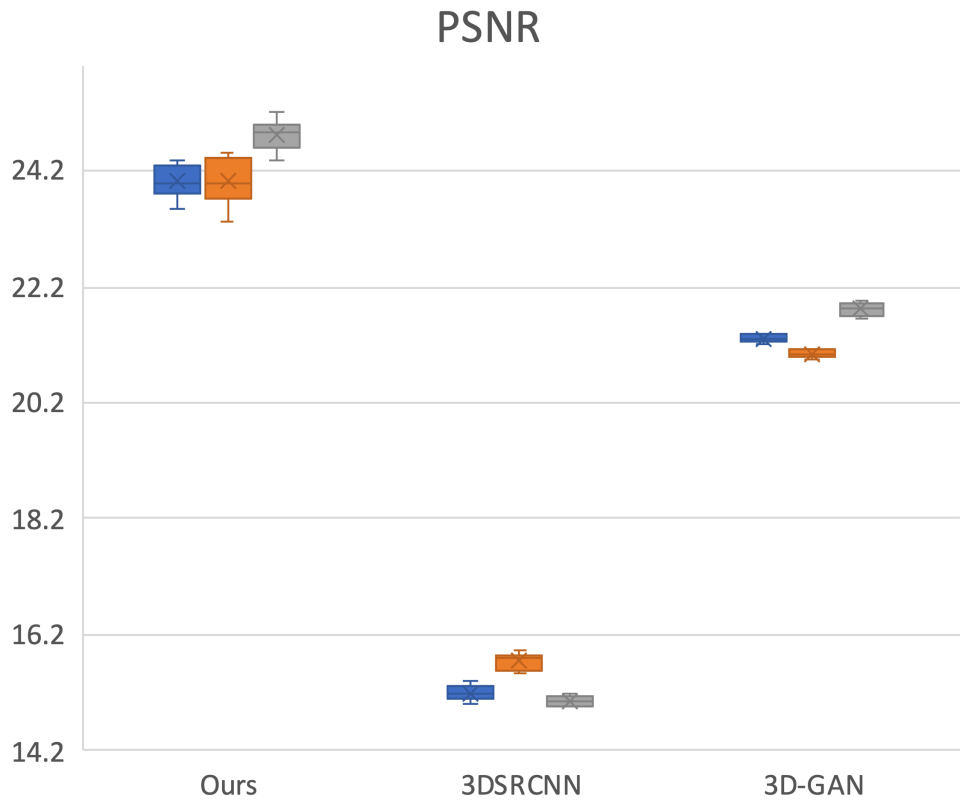

Fig. 4.5 Comparison of PSNR between 3D methods and the proposed method.

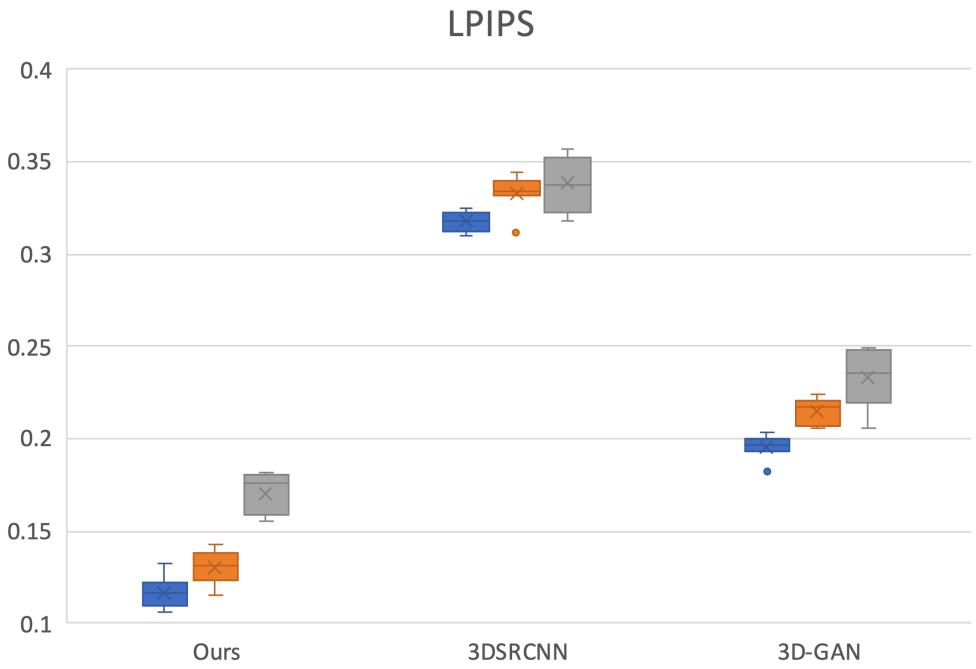

Fig. 4.6 Comparison of LPIPS between 3D methods and the proposed method.

4.4 Discussion

Our experiment is based on the direction of the two-dimensional slice to carry out the super-resolution reconstruction of the three-dimensional MRI, which realizes the simulation and reconstruction of the three-dimensional convolutional neural network. Based on the uniqueness of MRI, our method adopts the idea of two-step super-resolution reconstruction (Figure 2.5). The first reconstruction is responsible for obtaining more high-frequency information. The second reconstruction is responsible for restoring the corresponding semantic information and missing values to achieve a high-resolution MRI with excellent visual and image evaluation. Traditional deep learning super-resolution methods mostly use paired images for training and reconstruction. The experiment uses the medical image processing library to prepare the paired data set of MRI. In addition, we conduct simulations of four degradation mechanisms in the experiment. Table 4.4 shows the reconstruction of four low-resolution MRI by our method.

Our method performs better in Gaussian blur and noise but not as good as the former in the degraded mode of motion blur.

Within limited conditions, we need better super-resolution reconstruction performance. It can be seen from figure 3.3 that our proposed RMAM-GAN is better than other advanced methods in detail texture and vision. Table 4.1 shows the superiority of RMAM-GAN in image evaluation indicators. Subsequently, based on the missing values and noise after the recombination, we propose nESRGAN to perform the second super-resolution reconstruction of the recombined MRI. In combination with figure 4.4, nESRGAN also achieves good reconstruction performance in texture details, superior to other methods.

Moreover, there are no problems such as artifacts. Table 4.2 also illustrates the superiority of nESRGAN in image evaluation. Figure 4.2 and figure 4.3 also show the pixel distribution and high-frequency distribution of nESRGAN, which fits the distribution of high-resolution MRI slices.

The RMAM module in RMAM-GAN can obtain fine details. Compared with RFB, it can also generate a larger feature map to capture more contextual information. Moreover, the Senet in RMAM can improve the super-resolution reconstruction performance without affecting the overall model parameters. It can be seen from table 4.1 and the figure 3.3 that RMAM performs better than other methods. In addition, table 3.5 shows the configuration comparison of multiple modules in nESRGAN. The addition of noise can indeed provide more high-frequency information, and the global residual module can reduce the loss of detail. Our method is based on a two-dimensional convolutional neural network and successfully achieves super-resolution reconstruction of three-dimensional MRI. In table 4.4, our method is superior to the three-dimensional convolutional neural network method in all aspects. Our method can reduce training costs and memory utilization by reconstructing MRI through a two-dimensional neural

network. It has specific significance in brain MRI pathological analysis and diagnosis under limited conditions.

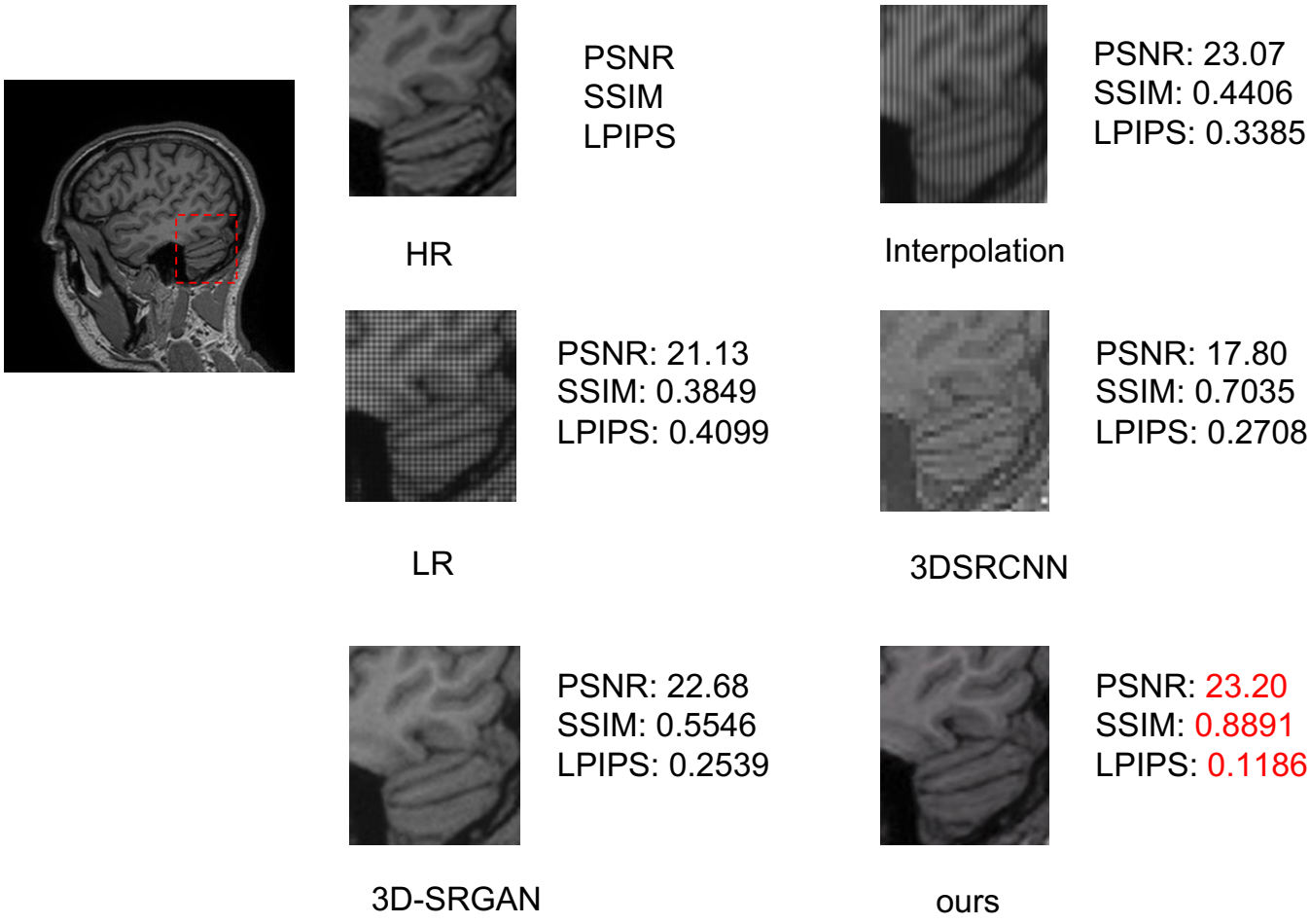

Fig. 4.7 Comparison of interpolation,3DSRCNN,3DSRGAN,and proposed method.

Table 4.3 Comparison of 2d and 3d methods on different datasets(mean ± standard deviation).

dataset		PSNR(dB) ↑	SSIM ↑	LPIPS ↓
IXI-dataset	Gaussian Blur	19.2471 ± 1.7245	0.4353 ± 0.0859	0.4661 ± 0.0268
	3D-SRCNN	16.5874 ± 0.3925	0.5352 ± 0.0273	0.4007 ± 0.0101
	3D-SRGAN	21.7050 ± 1.3896	0.7397 ± 0.0132	0.2021 ± 0.0113
	ours	**23.9249 ± 0.2631**	**0.8804 ± 0.0067**	**0.1220 ± 0.0043**
kenshin	Gaussian Blur	20.3414 ± 1.5248	0.4462 ± 0.0784	0.4335 ± 0.0234
	3D-SRCNN	16.5393 ± 0.5360	0.4085 ± 0.0639	0.4131 ± 0.0241
	3D-SRGAN	**24.5306 ± 1.0988**	0.6684 ± 0.0449	0.2471 ± 0.0162
	ours	24.2555 ± 0.2162	**0.8631 ± 0.0068**	**0.1354 ± 0.0058**
SiMon	Gaussian Blur	19.3083 ± 1.5396	0.3486 ± 0.0642	0.5203 ± 0.0219
	3D-SRCNN	15.7389 ± 0.5409	0.3326 ± 0.0401	0.4661 ± 0.0162
	3D-SRGAN	23.0346 ± 2.1304	0.5571 ± 0.0516	0.2345 ± 0.0263
	ours	**24.6393 ± 0.0844**	**0.8647 ± 0.0092**	**0.1681 ± 0.0133**

Table 4.4 The perfomance of different datasets by proposed method(mean ± standard deviation).

Dataset/Degredation		PSNR(dB) ↑	SSIM ↑	LPIPS ↓
IXI	Gassuian Blur	29.5049 ± 0.3803	0.8780 ± 0.0057	0.1461 ± 0.0098
	Gassuian Noise	26.1182 ± 0.1069	0.8353 ± 0.0067	0.1620 ± 0.0063
	Motion Blur	25.8653 ± 0.1223	0.8219 ± 0.0081	0.2172 ± 0.0074
	Motion Blur & noise	23.7876 ± 0.2120	0.7321 ± 0.0147	0.2575 ± 0.0129
Kenshin	Gassuian Blur	29.3052 ± 0.3746	0.8919 ± 0.0069	0.1403 ± 0.0108
	Gassuian Noise	25.7661 ± 0.3672	0.8693 ± 0.0070	0.1471 ± 0.0041
	Motion Blur	25.9764 ± 0.2049	0.8331 ± 0.0065	0.2095 ± 0.0047
	Motion Blur & noise	23.9465 ± 0.1187	0.7515 ± 0.0076	0.2337 ± 0.0044
Simon	Gassuian Blur	28.8848 ± 0.3795	0.8169 ± 0.0046	0.2063 ± 0.0054
	Gassuian Noise	25.5422 ± 0.3082	0.8158 ± 0.0135	0.2105 ± 0.0083
	Motion Blur	22.5868 ± 0.3551	0.7219 ± 0.0070	0.2928 ± 0.0077
	Motion Blur & noise	20.6202 ± 0.2197	0.5374 ± 0.0079	0.3789 ± 0.0059

Chapter 5

Conclusions and Prospects

In this chapter, we have conducted a summary of the research, and analyze related deficiencies and improvements, as well as the direction and ideas for future improvement.

5.1 Conclusions

In this paper, we propose a method based on a two-dimensional generative adversarial network to perform super-resolution reconstruction of 3DMRI. The experiment mainly design two networks for super-resolution reconstruction, namely RMAM-GAN and nESRGAN. By simulating the idea of a three-dimensional convolutional network and the volume characteristics of MRI, we use half the number of MRI slices for MRI super-resolution reconstruction, and then reorganize MRI. We adopt RMAM-GAN with RMAM module as the first super-resolution reconstruction network. After reorganizing the MRI, the nESRGAN of the noise module is used to further perform the feature restoration and detail supplement work of MRI. The result is a high-resolution brain MRI. Our experimental results show that our proposed method is better than the traditional MRI 3D convolutional neural network reconstruction method in terms of visual effects and image evaluation indicators. In general, our method realizes the three-dimensional super-resolution reconstruction of the brain MRI on the two-dimensional convolutional neural network. The reconstructed MRI can provide more details, and the diagnosis of brain pathology can provide certain help.

There are some shortcomings in the whole experiment:

1. In experiments, our method perform differently in different types of low-resolution MRI. Under the conditions of Gaussian blur and noise, the reconstructed MRI image is more realistic, but under the condition of dynamic blur, the performance is far inferior to the former. In addition, although the generation of the GAN is close to the original high-resolution image as a whole, there is a slight difference in brightness.

2. Experimental simulation of real-world low-resolution MRI still has many strength problems, and the characteristics of more low-resolution MRI are not considered. The robustness of the model still needs to be improved.

3. The experiment only uses the scaling factor of 2 to perform MRI super-resolution reconstruction, and does not perform multi-scale comparison. Although the RMAM module is suitable for multi-scale super-resolution reconstruction, the experiment did not compare the performance of super-resolution reconstruction at different scales.

5.2 Prospects

In the future experiments, we believe that there are still many improvements in the experiment. In the loss function, we use the combination of perceptual loss, content loss as the loss function of the network. However, the perceptual loss often considers the overall high-level features, ignoring some local features. Super-resolution reconstruction of MRI focuses more on detailed features. In the future, the loss function needs to be biased towards the direction and local characteristics of human perception. In addition, the paired datasets are often the inverse process of defining the image degradation process. The application of the network to natural MRI low-resolution images requires further research and improvement, and more unsupervised super-resolution directions need to be learned. The degradation method of the real image needs to be further

matched. In addition, we need to continue to supplement the comparison of 2D and 3D GPU usage and runtime.

Acknowledgement

Time flies, and I have already spent three years at the Kochi University of Technology before I realized it. Today, I am ready to graduate with a master's degree. I still remember the first time I stepped into the kami campus of the Kochi University of Technology as an exchange student three years ago. I liked the school atmosphere and campus environment very much. During this period, I have made many friends. The members in the laboratory are very friendly, and they have given me a lot of help in life and study. At that time, I made up my mind that I wanted to continue my studies at KUT and improve myself. In the past two years of study and research, I have gained a lot. In life, I learned how to adapt to the Japanese environment and how to communicate with others. In the study, I have made progress, and the accumulation of professional knowledge has improved my insights into the professional field and broadened my horizons.

To begin with, I would like to extend my sincere gratitude to my supervisor, Professor Yoshida Shinichi. He is an amiable and kind professor. I really like to discuss research with my professor, and every discussion with the professor has benefited me a lot. The learning outcomes in the period of graduate school are inseparable from his careful teaching and support. Special thanks to Professor Yoshida for giving me kind encouragement and helpful guidance in my papers' writing process. When I was preparing to attend conferences and journal papers, he spent a lot of time reading through each draft and provided me with good suggestions. There is an old Chinese saying that a teacher for a day is a father for a lifetime. I feel proud to be his student. It has been a great privilege and joy to study under his guidance and supervision. In addition, I am honored to benefit from his personality and hard work, which I will cherish for my

whole life. No one is perfect, and there is no end to learning. Always keep an upward heart. These are the philosophy of life that I learned from Professor Yoshida.

My sincere thanks are also given to my co-advisors, Professor Ren Xiangshi and Professor Matsuzaki Kiminori. Their valuable suggestions and incisive comments have helped significantly to the completion of the thesis.

I am also extremely grateful to every professor who gave the lesson during the two-year master's study. Their profound knowledge had greatly helped my study and made me learn a lot.

In addition, many thanks to all members of the laboratory for their help and support. The laboratory is always full of youthful spirit, and the atmosphere is very good. The positive learning atmosphere in the laboratory always makes me positive, constantly sharpening and improving. Furthermore, a special thanks to my friend who is one of the members of the laboratory, Yasuhiro Miura. He always helps me in life and encourages me to learn a lot of Japanese culture and knowledge. His optimism and sincerity always touch me and make me look forward to life. At the same time, we often discuss professional knowledge and culture to make progress together. I would also like to give my thanks to Post Doctor Shinomiya Yuki in the laboratory. Mr.Shinomiya also helped me a lot in my studies. He often gave me many research suggestions and guidance, which enabled me to learn a lot. I also sincerely thank Prof. Park Kaechang from Kochi Kenchin Clinic for his experimental support and help.

Special thanks to all the staff of KUT International Relations Center. Their care and help have given me a lot of support in life. Besides, I also thank my friends. They always listen to my voice and give me suggestions.

Lastly, my thanks would go to my beloved parents. It is their all-time care and love that has always supported me to continue to move forward. My parents are always silently standing by me behind my back, encouraging me, and letting me mature.

References

[1] Duyn, Jeff H. "The future of ultra-high field MRI and fMRI for study of the human brain." Neuroimage 62.2 (2012): 1241-1248.

[2] Pruessner, Jens C., Li Min Li, W. Serles, Marita Pruessner, D. Louis Collins, Noor Kabani, Sonia Lupien, and Alan C. Evans. "Volumetry of hippocampus and amygdala with high-resolution MRI and three-dimensional analysis software: minimizing the discrepancies between laboratories." Cerebral cortex 10, no. 4 (2000): 433-442.

[3] Soher, B.J.; Dale, B.M.; Merkle, E.M. A Review of MR Physics: 3T versus 1.5T. Magn. Reson. Imaging Clin. N. Am. 2006, 15, 277–290.

[4] Keihaninejad, Shiva, Rolf A. Heckemann, Gianlorenzo Fagiolo, Mark R. Symms, Joseph V. Hajnal, Alexander Hammers, and Alzheimer's Disease Neuroimaging Initiative. "A robust method to estimate the intracranial volume across MRI field strengths (1.5 T and 3T)." Neuroimage 50, no. 4 (2010): 1427-1437.

[5] Willinek, Winfried A., and Hans H. Schild. "Clinical advantages of 3.0 T MRI over 1.5 T." European journal of radiology 65, no. 1 (2008): 2-14.

[6] Park, Sung Cheol, Min Kyu Park, and Moon Gi Kang. "Super-resolution image reconstruction: a technical overview." IEEE signal processing magazine 20, no. 3 (2003): 21-36.

[7] Elad, M.; Feuer, A. Super-resolution reconstruction of image sequences. IEEE Trans. Pattern Anal. Mach. Intell. 1999, 21, 817–834.

[8] Pham, Chi-Hieu, Aurélien Ducournau, Ronan Fablet, and François Rousseau. "Brain MRI super-resolution using deep 3D convolutional networks." In 2017 IEEE 14th International Symposium on Biomedical Imaging (ISBI 2017), pp. 197-200. IEEE, 2017.

[9] Figueiredo, Oscar. "Advances in discrete geometry applied to the extraction of planes and surfaces from 3D volumes." PhD diss., Verlag nicht ermittelbar, 1999.

[10] Greenspan, Hayit, G. Oz, N. Kiryati, and S. L. B. G. Peled. "MRI inter-slice reconstruction using super-resolution." Magnetic resonance imaging 20, no. 5 (2002): 437-446.

[11] J. S. Isaac and R. Kulkarni, "Super resolution techniques for medical image processing," 2015 International Conference on Technologies for Sustainable Development (ICTSD), 2015, pp. 1-6, doi: 10.1109/ICTSD.2015.7095900.

[12] Plenge, Esben, Dirk HJ Poot, Monique Bernsen, Gyula Kotek, Gavin Houston, Piotr Wielopolski, Louise van der Weerd, Wiro J. Niessen, and Erik Meijering. "Super - resolution methods in MRI: can they improve the trade - off between resolution, signal - to - noise ratio, and acquisition time?." Magnetic resonance in medicine 68, no. 6 (2012): 1983-1993.

[13] Yang, Wenming, Xuechen Zhang, Yapeng Tian, Wei Wang, Jing-Hao Xue, and Qingmin Liao. "Deep learning for single image super-resolution: A brief review." IEEE Transactions on Multimedia 21, no. 12 (2019): 3106-3121.

[14] Glasner, D.; Bagon, S.; Irani, M. Super-resolution from a single image. In Proceedings of the 2009 IEEE 12th International Conference on Computer Vision, Kyoto, Japan, 29 September–2 October 2009; pp. 349–356.

[15] Wang, Z.; Chen, J.; Hoi, S.C.H. Deep learning for image super-resolution: A survey. IEEE Trans. Pattern Anal. Mach. Intell. 2020.

[16] Dong, Chao, Chen Change Loy, Kaiming He, and Xiaoou Tang. "Image super-resolution using deep convolutional networks." IEEE transactions on pattern analysis and machine intelligence 38, no. 2 (2015): 295-307.

[17] He, Kaiming, Xiangyu Zhang, Shaoqing Ren, and Jian Sun. "Deep residual learning for image recognition." In Proceedings of the IEEE conference on computer vision

and pattern recognition, pp. 770-778. 2016.

[18] Goodfellow, Ian, Jean Pouget-Abadie, Mehdi Mirza, Bing Xu, David Warde-Farley, Sherjil Ozair, Aaron Courville, and Yoshua Bengio. "Generative adversarial nets." Advances in neural information processing systems 27 (2014).

[19] Chen, Yuhua, Yibin Xie, Zhengwei Zhou, Feng Shi, Anthony G. Christodoulou, and Debiao Li. "Brain MRI super resolution using 3D deep densely connected neural networks." In 2018 IEEE 15th International Symposium on Biomedical Imaging (ISBI 2018), pp. 739-742. IEEE, 2018.

[20] Hongtao, Zhang, Yuki Shinomiya, and Shinichi Yoshida. "3D Brain MRI Reconstruction based on 2D Super-Resolution Technology." In 2020 IEEE International Conference on Systems, Man, and Cybernetics (SMC), pp. 18-23. IEEE, 2020.

[21] Karras, Tero, Samuli Laine, and Timo Aila. "A style-based generator architecture for generative adversarial networks." In Proceedings of the IEEE/CVF Conference on Computer Vision and Pattern Recognition, pp. 4401-4410. 2019.

[22] Odena, Augustus, Vincent Dumoulin, and Chris Olah. "Deconvolution and checkerboard artifacts." Distill 1, no. 10 (2016): e3.

[23] Liu, Songtao, and Di Huang. "Receptive field block net for accurate and fast object detection." In Proceedings of the European Conference on Computer Vision (ECCV), pp. 385-400. 2018.

[24] Shang, Taizhang, Qiuju Dai, Shengchen Zhu, Tong Yang, and Yandong Guo. "Perceptual extreme super-resolution network with receptive field block." In Proceedings of the IEEE/CVF Conference on Computer Vision and Pattern Recognition Workshops, pp. 440-441. 2020.

[25] Lan, Rushi, Long Sun, Zhenbing Liu, Huimin Lu, Cheng Pang, and Xiaonan Luo. "Madnet: A fast and lightweight network for single-image super resolution." IEEE transactions on cybernetics 51, no. 3 (2020): 1443-1453.

[26] Wang, Xintao, Ke Yu, Shixiang Wu, Jinjin Gu, Yihao Liu, Chao Dong, Yu Qiao, and Chen Change Loy. "Esrgan: Enhanced super-resolution generative adversarial networks." In Proceedings of the European conference on computer vision (ECCV) workshops, pp. 0-0. 2018.

[27] Zhang, Yulun, Yapeng Tian, Yu Kong, Bineng Zhong, and Yun Fu. "Residual dense network for image super-resolution." In Proceedings of the IEEE conference on computer vision and pattern recognition, pp. 2472-2481. 2018.

[28] Iandola, Forrest, Matt Moskewicz, Sergey Karayev, Ross Girshick, Trevor Darrell, and Kurt Keutzer. "Densenet: Implementing efficient convnet descriptor pyramids." arXiv preprint arXiv:1404.1869 (2014).

[29] Hu, Jie, Li Shen, and Gang Sun. "Squeeze-and-excitation networks." In Proceedings of the IEEE conference on computer vision and pattern recognition, pp. 7132-7141. 2018.

[30] Simonyan, Karen, and Andrew Zisserman. "Very deep convolutional networks for large-scale image recognition." arXiv preprint arXiv:1409.1556 (2014).

[31] Isola, Phillip, Jun-Yan Zhu, Tinghui Zhou, and Alexei A. Efros. "Image-to-image translation with conditional adversarial networks." In Proceedings of the IEEE conference on computer vision and pattern recognition, pp. 1125-1134. 2017.

[32] Jolicoeur-Martineau, Alexia. "The relativistic discriminator: a key element missing from standard GAN." arXiv preprint arXiv:1807.00734 (2018).

[33] Ronneberger, Olaf, Philipp Fischer, and Thomas Brox. "U-net: Convolutional networks for biomedical image segmentation." In International Conference on Medical image computing and computer-assisted intervention, pp. 234-241. Springer, Cham, 2015.

[34] Ledig, Christian, Lucas Theis, Ferenc Huszár, Jose Caballero, Andrew Cunningham, Alejandro Acosta, Andrew Aitken et al. "Photo-realistic single image super-

resolution using a generative adversarial network." In Proceedings of the IEEE conference on computer vision and pattern recognition, pp. 4681-4690. 2017.

[35] Hore, Alain, and Djemel Ziou. "Image quality metrics: PSNR vs. SSIM." In 2010 20th international conference on pattern recognition, pp. 2366-2369. IEEE, 2010.

[36] Zhang, Richard, Phillip Isola, Alexei A. Efros, Eli Shechtman, and Oliver Wang. "The unreasonable effectiveness of deep features as a perceptual metric." In Proceedings of the IEEE conference on computer vision and pattern recognition, pp. 586-595. 2018.

[37] IXI - Information eXtraction from images. www.brain-development.org

[38] Duchesne, Simon, Isabelle Chouinard, Olivier Potvin, Vladimir S. Fonov, April Khademi, Robert Bartha, Pierre Bellec et al. "The Canadian dementia imaging protocol: harmonizing national cohorts." Journal of Magnetic Resonance Imaging 49, no. 2 (2019): 456-465.

[39] Ali, Hanafy M. "MRI medical image denoising by fundamental filters." High-Resolution Neuroimaging-Basic Physical Principles and Clinical Applications 14 (2018): 111-124.

[40] Ali, Hanafy M. "MRI medical image denoising by fundamental filters." High-Resolution Neuroimaging-Basic Physical Principles and Clinical Applications 14 (2018): 111-124.

[41] Chen, Wensheng, Jie You, Bo Chen, Binbin Pan, Lihong Li, Marc Pomeroy, and Zhengrong Liang. "A sparse representation and dictionary learning based algorithm for image restoration in the presence of Rician noise." Neurocomputing 286 (2018): 130-140.

[42] Wang, Y., Teng, Q., He, X., Feng, J. and Zhang, T., 2019. CT-image of rock samples super resolution using 3D convolutional neural network. Computers δ Geosciences, 133, p.104314.

[43] Sánchez, Irina, and Verónica Vilaplana. "Brain MRI super-resolution using 3D generative adversarial networks." arXiv preprint arXiv:1812.11440 (2018).